Constitutive equations for the flow behavior of entangled polymeric systems: Application to star polymers

W. J. Briels,[1,a)] D. Vlassopoulos,[2] Kyongok Kang,[3] and Jan K. G. Dhont[3,a)]
[1]*Computational Biophysics, University of Twente, Postbus 217, 7500 AE Enschede, The Netherlands*
[2]*FORTH, Institute of Electronic Structure and Laser and Department of Materials Science and Technology, University of Crete, Heraklion 71110, Crete, Greece*
[3]*Forschungszentrum Jülich, IFF-7 Weiche Materie, D-52425 Jülich, Germany*

(Received 11 November 2010; accepted 3 February 2011; published online 22 March 2011)

A semimicroscopic derivation is presented of equations of motion for the density and the flow velocity of concentrated systems of entangled polymers. The essential ingredient is the transient force that results from perturbations of overlapping polymers due to flow. A Smoluchowski equation is derived that includes these transient forces. From this, an equation of motion for the polymer number density is obtained, in which body forces couple the evolution of the polymer density to the local velocity field. Using a semimicroscopic Ansatz for the dynamics of the number of entanglements between overlapping polymers, and for the perturbations of the pair-correlation function due to flow, body forces are calculated for nonuniform systems where the density as well as the shear rate varies with position. Explicit expressions are derived for the shear viscosity and normal forces, as well as for nonlocal contributions to the body force, such as the shear-curvature viscosity. A contribution to the equation of motion for the density is found that describes mass transport due to spatial variation of the shear rate. The two coupled equations of motion for the density and flow velocity predict flow instabilities that will be discussed in more detail in a forthcoming publication. © *2011 American Institute of Physics*. [doi:10.1063/1.3560616]

I. INTRODUCTION

Recently, the ever challenging nonlinear flow behavior of complex fluids has received renewed attention. This is due to advances in theoretical understanding as well as experimental instrumentation.[1–4] In particular, a number of experimental studies of polymeric systems have revealed the occurrence of shear banding along the gradient direction in such systems. For example, experiments on entangled DNA solutions[5,6] and solutions of synthetic polymers[7–9] show pronounced gradient-banding velocity profiles. It appears that the entanglements of polymeric chains are at the origin of the strong shear thinning behavior, which is necessary for gradient banding.[1] On the other hand, in recent experimental work with entangled synthetic polymers shear banding was not observed, but instead interfacial slip was suggested as the origin of strain loss.[10,11] Gradient banding has also been found in glassy starlike polymers.[12–14] Here, depending on the functionality and arm length of the star polymers, banding may be related to entanglements and/or to excluded volume interactions. Concerning the latter, there is growing evidence in the literature of shear banding phenomena in pasty materials.[15–17] On the other hand, again, some glassy colloids such as microgel pastes do not shear band.[18] Hence, the field remains controversial and widely open for interpretation.

From the above it becomes evident that the exact role of different parameters influencing the nonlinear rheology of soft matter systems remains in large elusive. In particular, concerning shear-gradient banding, it is unclear how generic the phenomenon is, and hence it is not possible to tailor it. So far there is no theory in which constitutive relations are derived on the basis of (semi-) microscopic considerations that include the nonlocal contributions that are essential to describe gradient banding. In the present paper we propose a semimicroscopic theory that should be able to explain shear-banding due to entanglement forces including coupling to concentration.

The importance of entanglements has been shown for star-branched copolymers in flow through narrow channels.[19] Moreover gradient banding in starlike grafted particles with overlapping (entangling) grafted chains has been found in a simulation study, in which the forces due to polymer entanglements were responsible for the observed banding.[20,21] The role of entanglements in shear-thinning behavior of polymers can be understood intuitively as follows. In strong flows, the dynamics of entangling and disentangling polymer chains occurs at about the same time scale as that of the shear-induced particle displacements (i.e., displacements of the center of mass of the whole particle); it is certainly not much faster. Therefore, the number of effective entanglements between two polymers is usually not equal to that in equilibrium. We note that the word "entanglement" is used here with a broader meaning to indicate a slowly relaxing topological constraint (of any kind) of two overlapping species (here polymers). In this respect, the "number of entanglements" should not be confused with the similar notion in classic tube theory,[22] although in some cases, linear long polymers, it is the same. The dynamics of entanglements as defined in this work is illustrated in the simulation snapshots of Fig. 1, taken from

a)Authors to whom correspondence should be addressed. Electronic mails: w.j.briels@utwente.nl and j.k.g.dhont@fz-juelich.de.

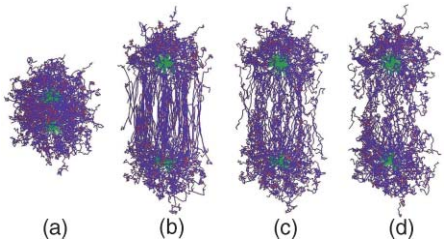

FIG. 1. (a) Two overlapping core–corona particles in equilibrium. The cores are depicted in green. (b) The positions of the particles immediately following a sudden increase of the distance between the cores. (c) A transient state where the particles rearrange toward equilibration. (d) The new equilibrated (steady) state.

Ref. 21 which describes the nonlinear rheology of particles with long grafted chains (of the core–corona type). Figure 1(a) depicts two such particles with overlapping coronas relaxed to equilibrium, with the cores (in green) kept fixed for a time that is long compared to the typical relaxation time of the coronas. In Fig. 1(b), the cores have suddenly been displaced. Instantly after the displacement, the number of entanglements of the coronas is equal to that before the displacement (i.e., initial equilibrium), and is larger than the number of entanglements that exists after equilibration (i.e., relaxation) has taken place at the new distance. This mismatch in the number of effective entanglements results in a transient attractive force between the cores, that relaxes to zero as the coronas equilibrate. Figure 1(c) corresponds to a transient state where the coronas are not yet fully relaxed, whereas in Fig. 1(d) the coronas have relaxed to the new equilibrium (steady) state. Similarly, there will be a transient repulsive force on suddenly decreasing the distance between the cores.

These entanglement-relaxation phenomena, which are also present in systems of very long linear polymers, such as those mentioned above, lead to strong shear thinning behavior: at low shear rates a large number of entanglements between two polymers exists, leading to a large viscosity, whereas at high shear rates there are very few entanglements since they have no time to redevelop when two polymers pass each other, leading to a low viscosity. Strong shear thinning is therefore expected to occur at shear rates equal to the inverse entanglement-disentanglement time. Note that tube-model theories can account for the fast flow-induced disentanglement leading to shear thinning (the so-called convected constraint release)[23] and associated shear banding.[24] In fact, a rather refined analysis of the shear-rate dependence of the release of entanglement constraints is now available based on these ideas,[25,26] although this issue is currently much under debate.

Given the broad concept of entanglements associated with the attractive forces outlined here, several other topological constraints can lead to similar shear thinning and banding phenomena. Indeed, another class of systems exhibiting similar flow behavior are telechelic and associating amphiphilic polymers (see, for example, Refs. 27–31). In these systems micelles are formed by the hydrophobic parts of block copolymers, bridged by their hydrophilic parts. In analogy to the changing number of entanglements in the polymeric systems, the number of bridges in a sheared associating system is not necessarily equal to their equilibrium values. This leads to similar transient forces and the accompanied strong shear-thinning behavior.

The theory developed in this paper is different from tube-model theories and is rather generic and can be equally applied to different systems, simply with an appropriate adjustment of the system- dependent parameters and functions appearing in the model.[21,32] Its key ingredient is the use of an evolution equation for the number of effective entanglements for developing constitutive equations. In addition, the diffusion equation for mass transport is derived, which couples to the Navier–Stokes equation. This approach allows to derive expressions for nonlocal contributions to the stress. In particular, an expression is obtained for the "shear-curvature viscosity" that is necessary to describe the interface in gradient banded systems. An alternative way to describe the interface is to introduce a "stress diffusion contribution" to the equation of motion for the stress tensor (see Refs. 33–36 for a discussion of both descriptions). In the present approach, we naturally find an expression for the stress tensor in terms of the shear-curvature viscosity. Furthermore, the origin of the shear-gradient-induced mass transport that plays a role in the diffusion equation is identified. The resulting coupling of shear-gradients and mass transport can lead to an instability that has been described by Schmitt *et al.*[37] We will refer to this instability as the "shear-concentration-coupling instability," or in abbreviation the SCC-instability. However, the origin of this instability is different from that of the gradient-banding instability. The coupled Navier–Stokes and diffusion equations derived in the present paper allow for an analysis of both instabilities, including nonlocal and nonlinear effects, as well as coupling to concentration.

Our approach, albeit generic, is applied to the particular case of star polymers. There are two reasons for this: First, star polymers represent an ideal soft colloidal model system, with a known, purely repulsive pair interaction potential that can be used.[37,38] Based on this potential, stars have been shown to be a tunable system interpolating between polymers and hard spheres depending on their functionality, and hence they are promising systems for addressing both entanglement and excluded volume topological constraints as discussed above.[39] Second, stars have been extensively studied and characterized experimentally and even velocity profile data already exist.[11–13]

The paper is organized as follows. In Sec. II, the coarse grained model that is at the basis of the theory is discussed. The equilibrium number of entanglements that is an input to the theory is considered in Sec. III. In Sec. IV, the Smoluchowski equation for the N-particle probability density function of the position coordinates and the number of entanglements is derived. From this Smoluchowski equation, the diffusion equation for the polymer concentration is derived in Sec. V. The diffusion equation turns out to be coupled to the body force that also appears in the Navier–Stokes equation. The various contributions to the body force are discussed in Sec. VI. One of these contributions is due to the entanglement forces, which are discussed in Sec. VII. In the same section explicit expressions are obtained for various (local and nonlocal) rheological response functions due to entangle-

ments. Contributions to the body force from potential forces, which are important at high shear rates, are considered in Sec. VIII. In Sec. IX, all contributions are collected and reviewed. Then, a few remarks concerning possible flow instabilities are made in Sec. X. In Sec. XI, we present some preliminary experiments with star polymers that exhibit gradient banding, pointing to the crucial role of entanglements in shear-gradient banding. Finally, Sec. XII provides a summary and conclusions.

II. A COARSE GRAINED MODEL

When modeling the dynamics of star particles, two processes are of importance: the dynamics of the centers-of-mass $\{\mathbf{R}_i\}$, $i = 1, 2, \ldots, N$ of the N stars and the internal dynamics of the coronas. Coronas of interacting stars in shear flow are generally not in equilibrium. Shear-induced perturbations of the coronas lead to additional forces between the stars, in addition to the thermodynamic forces. The associated additional elastic energy of stars i and j will be quantified by means of the deviation of a variable n_{ij} from its equilibrium value $n_0(R_{ij})$ at the prevailing distance R_{ij} between the two stars. The new variable n_{ij} will be interpreted as "the number of entanglements" or "the number of stickers" between polymers of the coronas of the two stars.[40] For brevity we shall refer to n_{ij} simply as "the number of entanglements." The dynamics of these entanglements is not much faster than the dynamics of the centers-of-mass, which leads to transient forces and memory effects, even on the two-particle level, as was discussed on an intuitive level in the introduction. Clearly, the transient elastic energy E_{ij} stored in the coronas will be a function of $n_{ij} - n_0(R_{ij})$. Since for the above mentioned attractive as well as repulsive transient forces, the transient energy is positive, the simplest form for the stored nonequilibrium energy is

$$E_{ij} = \frac{1}{2}\alpha[n_{ij} - n_0(R_{ij})]^2, \tag{1}$$

where the material constant α will be referred to as "the entanglement strength." This is an additional contribution to the free energy of the coronas when they are not in equilibrium, that is, when $n_{ij} \neq n_0(R_{ij})$. Alternatively, this form may be interpreted as the leading term in a formal expansion of E_{ij} with respect to $n_{ij} - n_0(R_{ij})$. This expression for the entanglement energy ensures that the configurational probabilities of the interacting stars are not affected by the transient forces, which was the motivation in Refs. 40 and 41 to introduce Eq.(1). The transient force $\mathbf{F}_{ij}$ of star j on star i, due to brush overlap, is thus equal to (with $\mathbf{R}_{ij} = \mathbf{R}_i - \mathbf{R}_j$)

$$\mathbf{F}_{ij} = -\nabla_i E_{ij} = \alpha[n_{ij} - n_0(R_{ij})]\frac{dn_0(R_{ij})}{dR_{ij}}\frac{\mathbf{R}_{ij}}{R_{ij}}. \tag{2}$$

Since $dn_0(R_{ij})/dR_{ij} < 0$, this reproduces the correct direction of the transient force as intuitively expected from Fig. 1. The total potential energy of the system of N stars can thus be written as

$$\Phi = \sum_{(i<j)=1}^{N}\left[V(R_{ij}) + \frac{1}{2}\alpha[n_{ij} - n_0(R_{ij})]^2\right], \tag{3}$$

where V is the pair-interaction potential between the stars that would exist when the coronas are in equilibrium for prescribed positions of the cores. The dynamics of the number of entanglements, with the neglect of thermal fluctuations, will be assumed to be single exponential with an "entanglement relaxation time" τ,

$$\frac{dn_{ij}}{dt} = -\frac{n_{ij} - n_0(R_{ij})}{\tau} = -\frac{1}{\alpha\tau}\frac{\partial\Phi}{\partial n_{ij}}, \tag{4}$$

where in the second expression we used Eq. (3) for the total energy Φ. This simple form for the relaxation of the number of entanglements accounts for the transient nature of the entanglement forces.[40,41]

Within the coarse-grained model, the degrees of freedom are the center-of-mass $\{\mathbf{R}_i\}$ of the cores and the number of entanglements $\{n_{ij}\}$. The appropriate equation of motion for the probability density function of these stochastic variables is discussed in Sec. IV. In the subsequent section we shall first discuss an approximation for the number n_0 of equilibrium entanglements.

III. THE EQUILIBRIUM NUMBER n_0 OF ENTANGLEMENTS

An intuitively appealing definition of the number of entanglements for a given distance R between two stars is the spatially integrated product of the number densities ρ_m of monomers from the two stars at each point,[40]

$$n_0 \sim \int d\mathbf{r}\,\rho_m(r_1)\rho_m(r_2) = 2\pi\int_{-1}^{1}dx\int_0^\infty dr\,r^2\rho_m(r) \times \rho_m(\sqrt{r^2 + R^2 - 2rRx}), \tag{5}$$

where r_1 and r_2 are the distance from the point $\mathbf{r}$ to the centers of each of the two stars. Entanglement forces will be important for low-functionality brushes in good solvents. For such stars there is a small core of radial size R_c where the monomer density is essentially constant. Up to a distance $R_k > R_c$, the Daoud–Cotton blob model[42] predicts a power dependence $\sim r^{-4/3}$. This scaling behavior of the monomer density has been confirmed both by simulations and by experiments. The distance R_k is referred to as "the corona radius." Beyond the corona, in the periphery of the star polymer, the monomer density is so low that it is proportional to the local osmotic pressure. This leads to the following expression for the normalized monomer density,[43,44]

$$\begin{aligned}\rho_m(r) &= 1, && \text{for } r < R_c,\\ &= \left(\frac{r}{R_c}\right)^{-4/3}, && \text{for } R_c \le r < R_k,\\ &= \frac{9}{17}\left(\frac{R_k}{R_c}\right)^{-4/3}\left[\frac{8}{9} + \left(\frac{R_k}{r}\right)^2\right]\exp\left\{-\frac{4}{9}\frac{r^2 - R_k^2}{R_k^2}\right\}, \\ &&& \text{for } R_k \le r.\end{aligned} \tag{6}$$

Numerical results for n_0 in Eq. (5), normalized to unity at zero separation, with the monomer density of Eq. (6) are given in Fig. 2, for two values of the core radius R_c. The solid line

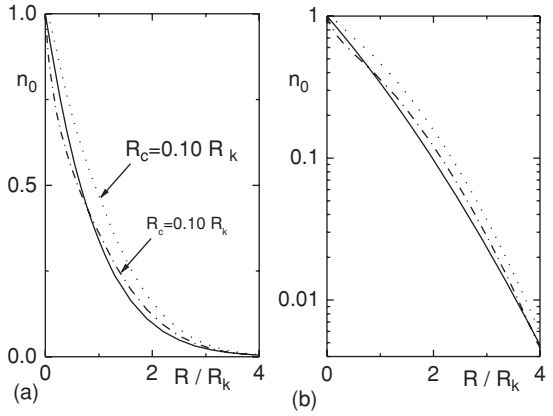

FIG. 2. (a) The normalized equilibrium number of entanglements n_0 as a function of the separation R between two stars in units of the corona radius R_k. The dotted line is for $R_c = 0.10R_k$ and the dashed-dotted line for $0.01\,R_k$. The solid line is the approximation in Eq. (2), with $\bar{n}$ set equal to unity. (b) The same plot on a logarithmic scale in order to emphasize the behavior of n_0 in the tail.

corresponds to the normalized form,

$$n_0(R) = \bar{n}\exp\{-R/R_k\}\exp\{-(R/R_k)^2/12\}, \tag{7}$$

which describes the numerical results quite satisfactorily for small values of the core radius R_c. Here, $\bar{n}$ is a measure for the equilibrium number of entanglements at full overlap of two coronas (which is taken to be unity in Fig. 2).

In the integrals in Eq. (5) we did not exclude core–core and core–brush overlaps. As a result, systems with larger cores will have an unphysically large n_0. As can be seen in Fig. 2, this is a small effect even for $R_c/R_k = 0.10$. In the remainder of this paper we therefore neglect this small effect, and use the expression (7) for n_0.

The various rheological response functions that we will calculate later depend on the core size R_c and the size of the corona R_k. It would be desirable to express R_c and R_k in terms of the experimentally known quantities like molecular weight of the arms, the functionality and the solvent quality. Such relations are discussed in Refs. 43 and 44. Apart from the radii R_c and R_k, rheological functions also depend on the dynamics of entanglements. As discussed in Sec. II, the dynamics of entanglements is characterized by the two parameters α and τ. As yet, little is known about the connection between these parameters and the microscopic quantities mentioned above.[40] This would require a separate study.

IV. THE SMOLUCHOWSKI EQUATION

The equation of motion for the probability density function (Pdf) $P(\{\mathbf{R}_i\},\{n_{ij}\},t)$ (with t the time) can be obtained[40] by a standard Kramers-Moyal expansion, starting from the Langevin equations that have been used in Refs. 41 and 45 to simulate concentrated suspensions of stars in flow. Instead of such a straightforward, but rather technically involved derivation, we shall here discuss an alternative derivation of this equation of motion.

The equation of motion for the Pdf is a conservation equation in phase space, spanned by the phase-space variables $\{\mathbf{R}_i\}$, $\{n_{ij}\}$, and is thus of the form,

$$\frac{\partial P}{\partial t} = -\sum_{i=1}^{N}\nabla_i\cdot\left[P\frac{d\mathbf{R}_i}{dt}\right] - \sum_{(i<j)=1}^{N}\frac{\partial}{\partial n_{ij}}\left[P\frac{dn_{ij}}{dt}\right], \tag{8}$$

where ∇_i is the gradient operator with respect to $\mathbf{R}_i$. The velocities $d\mathbf{R}_i/dt$ and dn_{ij}/dt must be expressed in terms of known function of the phase-space variables $\{\mathbf{R}_i\}$, $\{n_{ij}\}$ and the Pdf P in order to obtain a closed equation of motion. This is done in the overdamped limit, where the hydrodynamic friction force $\mathbf{F}_i^h$ on each star is balanced by direct interaction forces $-\nabla_i\Phi$, with Φ the total energy in Eq. (3), and the Brownian force $\mathbf{F}_i^{\mathrm{Br},c}$ that arises from coarse graining over the fast phase-space variables of the solvent,

$$\mathbf{0} = \mathbf{F}_i^h + \mathbf{F}_i^{\mathrm{Br},c} - \nabla_i\Phi. \tag{9}$$

Here, the superscript "c" stands for "cores," to indicate that this Brownian force is connected to the coarse-grained, overdamped dynamics of the position coordinates of the cores. With the neglect of hydrodynamic interactions, the friction force is equal to $-\xi[d\mathbf{R}_i/dt - \mathbf{v}(\mathbf{R}_i)]$, with ξ a friction coefficient and $\mathbf{v}$ the local suspension flow velocity.[46] Hence,

$$\frac{d\mathbf{R}_i}{dt} = -D\big[-\beta\mathbf{F}_i^{\mathrm{Br},c} + \beta\nabla_i\Phi\big] + \mathbf{v}(\mathbf{R}_i), \tag{10}$$

with $\beta = 1/k_{\mathrm{B}}T$, where k_{B} is Boltzmann's constant and T the temperature, and $D = k_BT/\xi$ is the translational diffusion coefficient of a star. For the overdamped dynamics of the number of entanglements, we similarly need to add a Brownian force $F_{ij}^{\mathrm{Br},e}$ to the force $-\partial\Phi/\partial n_{ij}$ in the right-hand side of Eq. (4),

$$\frac{dn_{ij}}{dt} = -D_e\left[-\beta F_{ij}^{\mathrm{Br},e} + \beta\frac{\partial}{\partial n_{ij}}\Phi\right], \tag{11}$$

where we shall refer to $D_e = k_BT/\alpha\tau$ as the "entanglement diffusion coefficient." The subscript "e" stands for "entanglements." Explicit expressions for the Brownian forces can be obtained by substitution of the Eqs. (10) and (11) into the conservation equation (8). In equilibrium, where $P \sim \exp\{-\beta\Phi\}$ and $\partial P/\partial t = 0$, it follows that the right-hand side of Eq. (8) vanishes when the Brownian forces take the form,

$$\begin{aligned}\mathbf{F}_i^{\mathrm{Br},c} &= -k_BT\nabla_i\ln P,\\ \mathbf{F}_{ij}^{\mathrm{Br},e} &= -k_BT\tfrac{\partial}{\partial n_{ij}}\ln P.\end{aligned} \tag{12}$$

In this way we arrive at the following equation of motion for the Pdf $P(\{\mathbf{R}_i\},\{n_{ij}\},t)$,

$$\begin{aligned}\frac{\partial P}{\partial t} = {}& D\sum_{i=1}^{N}\nabla_i\cdot[\nabla_iP + \beta P\nabla_i\Phi] - \sum_{i=1}^{N}\nabla_i\cdot[P\mathbf{v}]\\ &+ D_e\sum_{(i<j)=1}^{N}\frac{\partial}{\partial n_{ij}}\left[\frac{\partial}{\partial n_{ij}}P + \beta P\frac{\partial}{\partial n_{ij}}\Phi\right].\end{aligned} \tag{13}$$

This equation of motion is an extension of the well-known Smoluchowski equation for colloids, which now includes the degrees of freedom of the brushes. We will therefore refer to this equation as "the Smoluchowski equation."

There are three material constants involved in the Smoluchowski equation that are not a priori known: the translational diffusion constant D of noninteracting stars, the entanglements strength α, and the relaxation time τ [note that $D_e = k_B T/\alpha\tau$, and that α enters implicitly through the total potential Φ in Eq. (3)].

V. EQUATIONS OF MOTION FOR THE COLLOID DENSITY AND SUSPENSION FLOW VELOCITY

As will be seen, the equation for the suspension flow velocity couples to the number density $\rho(\mathbf{r}, t)$ of stars at position $\mathbf{r}$, which is defined as

$$\rho(\mathbf{r}, t) \equiv \left\langle \sum_{i=1}^{N} \delta(\mathbf{r} - \mathbf{R}_i) \right\rangle (t). \tag{14}$$

Here, the brackets $\langle \cdots \rangle$ stand for ensemble averaging with respect to the time-dependent probability density function $P(\{\mathbf{R}_i\}, \{n_{ij}\}, t)$ that was introduced in Sec. IV, and δ is the three-dimensional delta distribution. Let Γ denote the set of phase-space variables $\{\mathbf{R}_i\}$, $\{n_{ij}\}$ and $d\Gamma$ an infinitesimal volume element in this phase space. The time derivative of the macroscopic density can then be written as

$$\frac{\partial \rho(\mathbf{r}, t)}{\partial t} = \int d\Gamma \sum_{i=1}^{n} \delta(\mathbf{r} - \mathbf{R}_i) \frac{\partial P}{\partial t}, \tag{15}$$

where the integral ranges over the entire phase space. The right-hand side can now be evaluated by substitution of Eq. (13) for the time derivative of the Pdf. Without any further approximation it is readily found that,

$$\frac{\partial \rho}{\partial t} + \nabla \cdot [\rho \mathbf{v}] = D\nabla^2 \rho - \beta D \nabla \cdot \mathbf{B}, \tag{16}$$

where the body force $\mathbf{B}$ is defined as

$$\mathbf{B}(\mathbf{r}, t) = -\left\langle \sum_{i=1}^{N} [\nabla_i \Phi] \, \delta(\mathbf{r} - \mathbf{R}_i) \right\rangle (t). \tag{17}$$

The first term in the right-hand side in the equation of motion (16) describes the evolution of the density due to *free* diffusion, the second term accounts for mass transport due to interactions between the stars while the second term in the left-hand side accounts for changes of the density due to compression or dilatation. In the absence of flow, the body-force contribution can be shown to have the form $\Delta D \nabla^2 \rho$ (see, for example, Refs. 47 and 48). The free-diffusion contribution and the star–star interaction contribution can thus be lumped into a single term of the form $D^{\text{eff}} \nabla^2 \rho$, where $D^{\text{eff}} = D + \Delta D$, which renders Eq. (16) identical to Fick's law. The star–star interaction contributions are affected by flow, however, in a way that will be discussed in detail later.

The Navier–Stokes equation for the local suspension velocity can be written as

$$\rho_0 \left\{ \frac{\partial \mathbf{v}}{\partial t} + \mathbf{v} \cdot \nabla \mathbf{v} \right\} = \mathbf{B}, \tag{18}$$

where ρ_0 is the overall mass density of the polymer system. We will furthermore assume that the flow is incompressible,

$$\nabla \cdot \mathbf{v} = 0. \tag{19}$$

An explicit form for the body force will be derived in the remaining part of the paper, which closes the set of equations given above, and which then allows for an analysis of possible shear-induced instabilities.

VI. CONTRIBUTIONS TO THE BODY FORCE

The ensemble average in Eq. (17) for the body force is first written as a phase-space integral,

$$\mathbf{B}(\mathbf{r}, t) = -N(N-1) \int d\mathbf{r}' \int dn \, P(\mathbf{r}, \mathbf{r}', n, t) \nabla \left\{ V(|\mathbf{r} - \mathbf{r}'|) + \frac{1}{2} \alpha [n - n_0(|\mathbf{r} - \mathbf{r}'|)]^2 \right\}, \tag{20}$$

where,

$$P(\mathbf{R}_1, \mathbf{R}_2, n_{12}, t) = \int d\mathbf{R}_3 \cdots \int d\mathbf{R}_N \int dn_{13} \cdots \times \int dn_{N-1N} \, P(\{\mathbf{R}_i\}, \{n_{ij}\}, t), \tag{21}$$

is the probability density function for $\mathbf{R}_1$, $\mathbf{R}_2$, and n_{12}, with P the N-particle Pdf that was introduced in Sec. IV.

Performing the derivative we obtain three terms, two of which may be combined in order to write,

$$\mathbf{B}(\mathbf{r}, t) = \mathbf{B}_W(\mathbf{r}, t) + N(N-1)\alpha \int d\mathbf{r}' \int dn \, P(\mathbf{r}, \mathbf{r}', n, t) \times n \nabla n_0(|\mathbf{r} - \mathbf{r}'|), \tag{22}$$

with,

$$\mathbf{B}_W = -\rho(\mathbf{r}, t) \int d\mathbf{r}' \rho(\mathbf{r}', t) g(\mathbf{r}, \mathbf{r}', t) \nabla W(|\mathbf{r} - \mathbf{r}'|), \tag{23}$$

and

$$W = V + \frac{1}{2} \alpha n_0^2. \tag{24}$$

The pair-correlation g is defined as

$$P(\mathbf{r}, \mathbf{r}', t) = \int dn \, P(\mathbf{r}, \mathbf{r}', n, t) = \frac{1}{N(N-1)} \rho(\mathbf{r}, t) \rho(\mathbf{r}', t) g(\mathbf{r}, \mathbf{r}', t). \tag{25}$$

W may be considered as an effective potential. At very high shear rates particles pass each other too quickly to form any entanglements. In this case n may be taken to be zero and $\mathbf{B}_W$ is the only remaining term. The effect of adding $(1/2)\alpha n_0^2$ to the thermodynamic potential V is to effectively enlarge the diameter of the particles.

In order to calculate the second term in Eq. (22) we assume that Brownian motions may be neglected, even at the lowest shear rates, and that the entanglements n are to a good approximation given by the deterministic values $\hat{n}(\mathbf{r}, \mathbf{r}', t)$ obtained from the equation of motion (4) with R_{ij} set by the flow. The evaluation of $\hat{n}$ and a detailed discussion of entanglement forces are presented in Subsection VII A. The probability function in the second term of Eq. (22) is thus approx-

imated as

$$P(\mathbf{r}, \mathbf{r}', n, t) \approx P(\mathbf{r}, \mathbf{r}', t)\delta(n - \hat{n}(\mathbf{r}, \mathbf{r}', t)), \tag{26}$$

where δ is the delta distribution. As a second approximation, we assume that at low and intermediate shear rates the deformation of the pair-correlation in the second term of Eq. (22) is negligibly small. We stress that this assumption is only applied to the second term in Eq. (22). To understand the validity of this assumption, notice that at low shear rates both $g(r)$ and the average of $n - n_0$ deviate from their values at equilibrium by values proportional to $\dot{\gamma}$. Our assumption therefore implies that the constant of proportionality in the latter case is much larger than that in the former case. For stars with extended coronas, moreover, the pair-correlation function in equilibrium is approximately equal to unity. Therefore we assume that the pair-correlation function in the second term in Eq. (22) may be put equal to unity at low and intermediate shear rates. Since at high shear rates, where this approximation breaks down, the number of entanglements is essentially equal to zero, we may put the pair-correlation function in the second term of Eq. (22) equal to unity at *all* shear rates. Introducing the approximations just mentioned we find as our final equation for the body force,

$$\mathbf{B}(\mathbf{r}, t) = \mathbf{B}_W(\mathbf{r}, t) + \mathbf{B}_e(\mathbf{r}, t) + \mathbf{B}_0(\mathbf{r}, t), \tag{27}$$

with,

$$\mathbf{B}_e(\mathbf{r}, t) = \alpha\rho(\mathbf{r}, t) \int d\mathbf{r}'\rho(\mathbf{r}', t) \left[\hat{n}(\mathbf{r}, \mathbf{r}') - n_0(|\mathbf{r}-\mathbf{r}'|)\right] \times \nabla n_0(|\mathbf{r}-\mathbf{r}'|), \tag{28}$$

and,

$$\mathbf{B}_0(\mathbf{r}, t) = \frac{1}{2}\alpha\rho(\mathbf{r}, t) \int d\mathbf{r}'\rho(\mathbf{r}', t)\nabla n_0^2(|\mathbf{r}-\mathbf{r}'|). \tag{29}$$

The subscript "*e*" refers to "entanglements," and $\mathbf{B}_e$ will be referred to as "the entanglement body force."

This term will be considered in Sec. VII , while in Sec. VIII the body force $\mathbf{B}_W$ at high shear rates as well as $\mathbf{B}_0$ will be further analyzed.

VII. THE ENTANGLEMENT BODY FORCE $\mathbf{B}_e$

In this section we will analyze the body force that originates from entanglements. Entanglement forces will be discussed in Subsection VII A. An expression for the resulting body force is derived in Subsection VII B in terms of spatial integrals of the entanglement force. On the basis of this formal expression, various viscoelastic response functions are defined in Subsection VII C, for which explicit results, including their shear-rate dependence, will be given in Subsection VII D.

The assumption in the analysis in this section is that gradients in the local shear rate and density exist in one direction, which is chosen as the y-direction. The local suspension velocity is chosen in the x-direction.

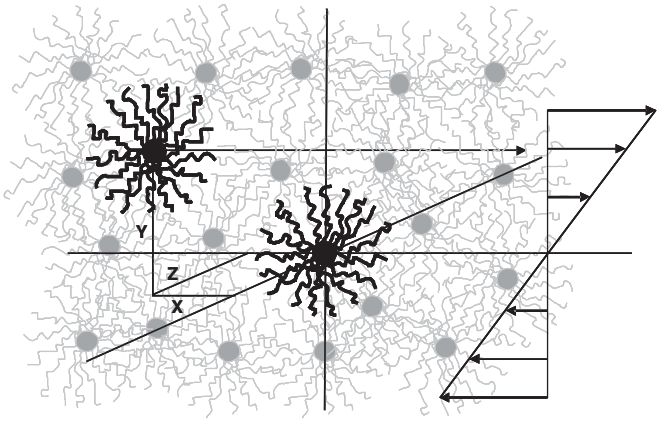

FIG. 3. The average path of a given star (the bold-faced drawn star in the left upper region) relative to another star at the origin (also bold faced) is approximately a straight line as indicated by the arrow.

A. Entanglement forces

Consider two star polymers (the two bold-face stars in Fig. 3) in a homogeneous system, where one of the stars is positioned at the origin. The local stationary flow direction is chosen in the x-direction, the gradient direction is along y while z is the vorticity direction. The two stars are forced to interact while passing each other as a result of the imposed shear flow and the interactions with the remaining stars. Under the influence of interaction forces by surrounding stars, the path that the moving star follows is in good approximation a straight line. The position coordinate of the moving star is thus equal to

$$\mathbf{R}(t) = (X = v(Y)t, Y, Z), \tag{30}$$

where (X, Y, Z) is the position of the moving star, and $v(Y)$ is its velocity in x-direction relative to the star at the origin. For a constant shear rate, independent of position, the velocity is simply equal to $v(Y) = Y\dot{\gamma}$. Note that $t = 0$ is chosen as the time that the moving star is right above the star at the origin, that is, when the x-coordinate of the moving star is zero.

The entanglement force that the moving star exerts on the star at the origin is equal to

$$\mathbf{F} = -\alpha\,[\hat{n} - n_0]\,\nabla n_0(R), \tag{31}$$

where the gradient operator is with respect to $\mathbf{R}$ (which is equal to $\mathbf{r}' - \mathbf{r}$ in terms of the coordinates used in Sec. VI). The number of entanglements $\hat{n}$ is found by integration of Eq. (4), with n_{ij} taken equal to $\hat{n}$,

$$\hat{n} = \frac{1}{\tau}\int_{-\infty}^{t} dt' n_0(R(t'))\exp\{-(t - t')/\tau\}. \tag{32}$$

The times t and t' can be written in terms of x-coordinates using Eq. (30), leading to

$$\hat{n} = \frac{1}{v(Y)\tau}\exp\left\{-\frac{X}{v(Y)\tau}\right\}\int_{-\sigma\infty}^{X} dX' n_0(R')\exp\left\{\frac{X'}{v(Y)\tau}\right\}, \tag{33}$$

where σ is the sign of Y and $R' = \sqrt{X'^2 + Y^2 + Z^2}$. According to Eqs. (31) and (33), the force on the star at the origin

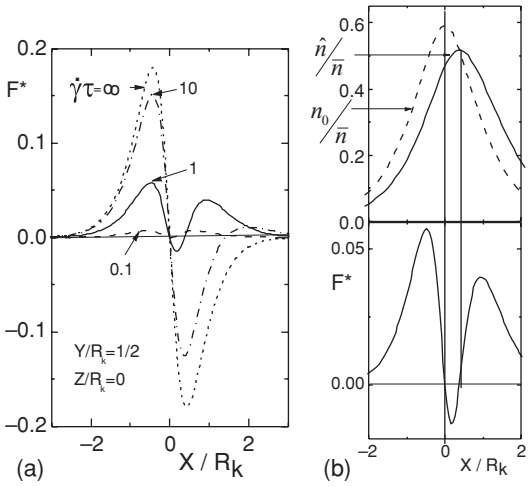

FIG. 4. (a) The entanglement force in Eq. (34) in dimensionless form $F^\star = FR_k/\alpha$ as a function of X/R_k for $\dot\gamma\tau = 0.1$ (dashed line), 1 (solid line), 10 (dashed-dotted line), and ∞ (the short-dashed line). The y- and z-coordinates are equal to $Y = R_k/2$ and $Z = 0$, respectively. (b) The equilibrium number of entanglements n_0 (the dashed line in the upper figure) and the actual number of entanglements n (the solid line) for $Y = R_k/2$ and $Z = 0$, and a shear rate equal to $\dot\gamma\tau = 1$. The lower figure is the force [the same as in (a)]. The vertical lines mark the points where $X = 0$ and where $n - n_0$ changes sign.

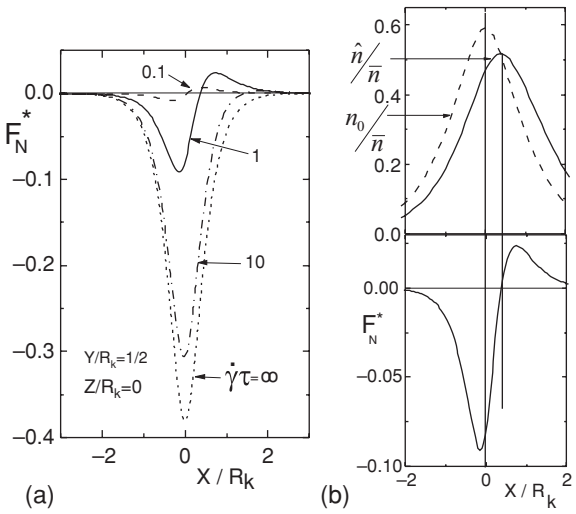

FIG. 5. Same as in Fig. 4, but now for the normal force. (a) The dimensionless form $F_N^\star = FR_k/\alpha$ of the normal force in Eq. (34) as a function of X/R_k for $\dot\gamma\tau = 0.1$ (dashed line), 1 (solid line), 10 (dashed-dotted line), and ∞ (the short-dashed line). The y- and z-coordinates are equal to $Y = R_k/2$ and $Z = 0$, respectively. (b) The equilibrium number of entanglements n_0 (the dashed line in the upper figure) and the actual number of entanglements n (the solid line) for $Y = R_k/2$ and $Z = 0$, and a shear rate equal to $\dot\gamma\tau = 1$. The lower figure is the force [the same as in (a)]. The vertical lines mark the points where $X = 0$ and where $\hat n - n_0$ changes sign.

due to entanglement forces is thus given by

$$\mathbf{F} = -\frac{\alpha}{v(Y)\tau}\frac{dn_0(R)}{dR}\frac{\mathbf{R}}{R}\exp\left\{-\frac{X}{v(Y)\tau}\right\}\int_{-\sigma\infty}^{X} dX' \times[n_0(R') - n_0(R)]\exp\left\{\frac{X'}{v(Y)\tau}\right\}. \quad (34)$$

Substitution of the explicit form (7) for the equilibrium number of entanglements allows an explicit calculation of the entanglement forces. The entanglement forces along the flow direction and in the normal direction are plotted in Figs. 4 and 5.

First consider the force along the flow direction plotted in Fig. 4. The velocity $v(Y)$ is taken to be given by $v(Y) = \dot\gamma Y$, i.e., as for homogeneous shear flow. The plot in Fig. 4 refers to a moving star in the positive x direction with a fixed y coordinate equal to half the corona size R_k and with $z = 0$ (see Fig. 3). The force that is plotted is the force exerted by the moving star on a star fixed at the origin. For very low shear rates, such that $\dot\gamma\tau \ll 1$, the actual number of entanglements is almost always equal to its equilibrium value, so the entanglement forces are very weak. On increasing the shear rate, the formation of entanglements cannot keep up with the changing equilibrium values [this is illustrated in Fig. 4(b)]. As a result, the star at the origin is pushed along the positive x axis when the moving star approaches the star at the origin from the left. Since the actual number of entanglements is less than its equilibrium value, the forces are such as to move stars to positions where the equilibrium value of entanglements is equal to the actual number of entanglements. When the moving star is at $x = 0$, above the star at the origin, the force along the x direction is zero because $dn_0(R)/dR = 0$. On continuing along the positive x axis, the moving star repels the star at the origin toward the negative x direction for the same reasons mentioned above. Since the stars now move away from each other, so that n_0 decreases, there will be a point where $n = n_0$. Beyond this point the actual number of entanglements is larger than its equilibrium value, so the stars attract each other, that is, the moving star drags along the star at the origin. This implies that the force is positive again. For very high shear rates the actual number of entanglements is essentially zero. The remaining force is now equal to $\alpha n_0 \nabla n_0$. This is the antisymmetric short-dashed curve in Fig. 4(a), where the narrow interval of negative forces disappeared.

The normal force in the positive y direction (the gradient direction) is plotted in Fig. 5. On approach from the left, the star at the origin is pushed down in the direction of larger separation, for precisely the same reason as discussed above. Beyond the point where $\hat n = n_0$ [see Fig. 5(b)], the stars attract each other again, resulting in a positive normal force.

B. The body force

The entanglement body force in Eq. (28) at the origin is most conveniently expressed in terms of the instantaneous entanglement force $\mathbf{F}$ that the moving star exerts on the star at the origin,

$$\mathbf{B}_e = \rho(\mathbf{r} = \mathbf{0})\int d\mathbf{R}\rho(Y)\mathbf{F}, \quad (35)$$

where the entanglement force $\mathbf{F}$ is given in Eq. (34). Note that for the stationary shear under consideration, the body forces are independent of time. For distances between two stars within the range of interaction, the velocity $v(Y)$ in Eq. (34) for the force can be expressed in terms of the local

shear rate $\dot{\gamma}$ and its spatial derivatives as,

$$\begin{aligned} v(Y) &= \int_0^Y dY' \dot{\gamma}(Y') \\ &= \int_0^Y dY' \left[\dot{\gamma} + Y' \frac{d\dot{\gamma}}{dY} + \frac{1}{2} Y'^2 \frac{d^2\dot{\gamma}}{dY^2} + \frac{1}{6} Y'^3 \frac{d^3\dot{\gamma}}{dY^3} \right] \\ &= Y[\dot{\gamma} + \Delta(Y)], \end{aligned} \tag{36}$$

with,

$$\Delta(Y) = \frac{1}{2} Y \frac{d\dot{\gamma}}{dY} + \frac{1}{6} Y^2 \frac{d^2\dot{\gamma}}{dY^2} + \frac{1}{24} Y^3 \frac{d^3\dot{\gamma}}{dY^3}. \tag{37}$$

Here and in the sequel, when the position dependence of the density, shear-rate and spatial derivatives is not explicitly denoted, their local values at the origin are meant. As will be seen later, the reason for including the third order spatial derivative of the shear rate in Eq. (36) is that this term is essential to describe the interface in a shear-banded state. This contribution is related to the nonlocal terms in the constitutive relations discussed in Refs. 33–36 in connection to gradient-shear banding.

When gradients are smooth on the length scale set by the range of interactions between the stars, the integrand in Eq. (35) can be expanded in a Taylor series with respect to Y up to order Y^3. A somewhat lengthy calculation that is given in Appendix A leads to

$$\mathbf{B}_e = \frac{\partial}{\partial Y} \left[\frac{1}{2} \rho^2 \mathbf{I}_1 + \frac{1}{24} \rho^2 \frac{\partial^2 \dot{\gamma}}{\partial Y^2} \frac{d\mathbf{I}_3}{d\dot{\gamma}} + \frac{1}{6} \rho \frac{\partial^2 \rho}{\partial Y^2} \mathbf{I}_3 \right], \tag{38}$$

where the vector integrals are defined as,

$$\begin{aligned} \mathbf{I}_1 &= \int d\mathbf{R} Y \mathbf{F}(\mathbf{R} \,|\, \dot{\gamma}), \\ \mathbf{I}_3 &= \int d\mathbf{R} Y^3 \mathbf{F}(\mathbf{R} \,|\, \dot{\gamma}). \end{aligned} \tag{39}$$

Here, $\mathbf{F}(\mathbf{R} \,|\, \dot{\gamma})$ is the force in Eq. (34) with $v(Y) = Y\dot{\gamma}$, and ρ, $\dot{\gamma}$, and their spatial derivatives are understood to be taken at the origin. The first term in the right-hand side of Eq. (38) complies with the general expression $-(1/2V)\sum_{i,j} \mathbf{R}_{ij}\mathbf{F}_{ij}$ for the stress tensor (where V is the volume of the system, $\mathbf{R}_{ij}$ is the distance between particles i and j, and $\mathbf{F}_{ij}$ is the force of particle i on j). The second and third terms are "nonlocal" contributions. In particular the last term is essential to describe the interface in a gradient-banded state.

C. Rheological response functions

The expression (38) for the entanglement body force can be rewritten as

$$\begin{aligned} \mathbf{B}_e = \frac{\partial}{\partial Y} \Bigg[&\left\{ \dot{\gamma}\eta_e - \frac{\partial^2 \dot{\gamma}}{\partial Y^2} \kappa + \dot{\gamma} \frac{\partial^2 \rho}{\partial Y^2} \chi \right\} \hat{\mathbf{e}}_x \\ &+ \dot{\gamma} \left\{ \dot{\gamma} N + \frac{\partial^2 \dot{\gamma}}{\partial Y^2} \kappa_N + \dot{\gamma} \frac{\partial^2 \rho}{\partial Y^2} \chi_N \right\} \hat{\mathbf{e}}_y \Bigg], \end{aligned} \tag{40}$$

where the various response functions can be obtained from the definitions of the integrals in Eq. (39).

The explicit expression for the "entanglement viscosity" that follows from Eq. (38) reads,

$$\eta_e(\rho, \dot{\gamma}) = \frac{1}{2} \frac{\rho^2}{\dot{\gamma}} \int d\mathbf{R} Y F_x(\mathbf{R} \,|\, \dot{\gamma}), \tag{41}$$

The index "e" on the viscosity is used here to indicate that this is the contribution to the total viscosity that is due to entanglement forces, and the index "x" on the force denotes its x-component.

By symmetry, the normal forces due to entanglements in the z-direction are zero. Furthermore, body forces due to normal stresses along the flow direction do not contribute due to the assumed homogeneity in that direction. There is a nonzero stress contribution related to the normal force in the y-direction. According to Eq. (38), the normal-stress coefficient N in the gradient direction is equal to

$$N(\rho, \dot{\gamma}) = \frac{1}{2} \frac{\rho^2}{\dot{\gamma}^2} \int d\mathbf{R} Y F_y(\mathbf{R} \,|\, \dot{\gamma}), \tag{42}$$

where F_y is the entanglement force in the y-direction.

In addition to the "standard" contributions to the stress, the nonlocal contributions are important when describing flow instabilities. There is a shear-stress contribution that has been introduced phenomenologically in Refs. 33–36 in order to describe the interface in a gradient-banded state. This contribution corresponds to the second term in Eq. (38) and defines the "shear-curvature viscosity" κ,

$$\kappa(\rho, \dot{\gamma}) = -\frac{1}{24} \rho^2 \frac{d}{d\dot{\gamma}} \int d\mathbf{R} Y^3 F_x(\mathbf{R} \,|\, \dot{\gamma}). \tag{43}$$

A minus sign is added to the definition of the shear-curvature viscosity, since this should render κ positive, as discussed in Ref. 33. An alternative way to describe the interface in a gradient-banded state has been introduced by Olmsted,[34,49] by adding a diffusive contribution to an equation of motion for the stress tensor. The corresponding phenomenological coefficient is commonly referred to as "the stress-diffusion coefficient." Within the present approach, the nonlocal contribution arises simply from an extended Taylor expansion of the body force (i.e., the stress tensor), including higher order spatial derivatives. This complies with the phenomenologically approach taken from Refs. 33–36.

The nonlocal normal stress arising from the second term in Eq. (38) for the body force is written in terms of the "nonlocal normal-stress coefficient" κ_N,

$$\kappa_N(\rho, \dot{\gamma}) = \frac{1}{24} \frac{\rho^2}{\dot{\gamma}} \frac{d}{d\dot{\gamma}} \int d\mathbf{R} Y^3 F_y(\mathbf{R} \,|\, \dot{\gamma}), \tag{44}$$

where the subscript N refers to normal forces. This contribution describes normal stresses that arise from large spatial gradients in the shear rate, similar to the nonlocal contribution in Eq. (43) for shear stresses.

The last term in Eq. (38) describes nonlocal contributions due to density inhomogeneities. The stress arising from density inhomogeneities in the flow direction can be formulated in terms of what we will refer to as "the shear-concentration coupling parameter" χ,

$$\chi(\rho, \dot{\gamma}) = \frac{1}{6} \frac{\rho}{\dot{\gamma}} \int d\mathbf{R} Y^3 F_x(\mathbf{R} \,|\, \dot{\gamma}), \tag{45}$$

while the corresponding coefficient χ_N for the stress along the normal direction is

$$\chi_N(\rho, \dot{\gamma}) = \frac{1}{6} \frac{\rho}{\dot{\gamma}^2} \int d\mathbf{R} Y^3 F_y(\mathbf{R} \,|\, \dot{\gamma}), \tag{46}$$

which will be referred to as "the normal-force concentration-coupling parameter."

D. Shear-rate dependence of the response functions

In this subsection, the integral representations of the various rheological response functions as given in Subsection VII C, will be numerically evaluated, and accurate Padé approximations will be given which makes their shear-rate dependence explicit. In addition, all expressions will be written in dimensionless variables.

The dimensionless concentration φ and the "entanglement stress" S are defined as

$$\begin{aligned} \varphi &= \rho/\rho^\star = c/c^\star, \\ S &= \frac{1}{9}\rho^{\star 2}\alpha\bar{n}^2 R_k^3. \end{aligned} \tag{47}$$

where,

$$\rho^\star = \frac{3}{4\pi} R_k^{-3}, \tag{48}$$

is the overlap number concentration, that is, the concentration where the volume fraction of spheres with radius R_k is unity, and $c^\star$ is the corresponding overlap concentration in arbitrary units (such as mg/ml). Note that an obvious experimental length scale to calculate the volume fraction is the hydrodynamic radius rather than R_k. In comparing with experiments, one should therefore establish a relation between the hydrodynamic radius and R_k, which is an issue that we will not address here. The various rheological response functions are conveniently written as

$$\begin{aligned} &\eta_e = \frac{9}{2}\tau S\varphi^2\Gamma_\eta, \quad N = \frac{9}{2}\tau^2 S\varphi^2\Gamma_N, \quad \kappa = \frac{3}{8}R_k^2\tau S\varphi^2\Gamma_\kappa, \\ &\kappa_N = \frac{3}{8}R_k^2\tau^2 S\varphi^2\Gamma_{\kappa_N}, \quad \chi = \pi R_k^5\tau S\varphi\Gamma_\chi, \\ &\chi_N = \pi R_k^5\tau^2 S\varphi\Gamma_{\chi_N}, \end{aligned} \tag{49}$$

where the dimensionless Γ's describe the shear-rate dependence of the response functions, which are given by (with $x = \dot\gamma\tau$)

$$\begin{aligned} \Gamma_\eta(x) &= \frac{73}{5}\frac{4+x^2}{[26+x^2][5+7x^2]}, \\ \Gamma_N(x) &= -\frac{50}{3}\frac{4+x^2}{[100+8x^2][1+2x^2]}, \\ \Gamma_\kappa(x) &= -\frac{87}{10}\frac{10-9x^2}{[10+x^2][10+75x^2]}, \\ \Gamma_{\kappa_N}(x) &= -\frac{440}{[100+35x^2]\sqrt{1+22x^2}}, \\ \Gamma_\chi(x) &= \frac{220[5+11x^2][20+x^2]}{[5+23x^2][50+29x^2][100+3x^2]}, \\ \Gamma_{\chi_N} &= -219\frac{10+26x^2}{[10+72x^2][100+53x^2]}. \end{aligned} \tag{50}$$

As can be seen from Eqs. (49) and (50), $\dot\gamma\eta_e \approx S$ for $\dot\gamma = 1/\tau$ and $\rho = \rho^\star$. Hence, S in Eq. (47) is the shear stress due to entanglement forces at a shear rate equal to $\dot\gamma = 1/\tau$ and a concentration equal to $\rho^\star$. This is why the numerical factor 1/9 is chosen in Eq. (47) for S. The numerical evaluation of the integrals that represent the various rheological response functions (see Subsection VII C) and their approximations by the Padé approximants in Eq. (50) are discussed in Appendix B. The numerical results for the integrals are the dashed-dotted lines in Fig. 6, while the solid lines correspond to the Padé approximants. The Padé approximants are constructed such that they describe the asymptotic behavior of the response functions at small and high shear rate correctly, and are accurate to within a few percent for intermediate shear rates.

VIII. HIGH SHEAR-RATE RESPONSE

As discussed in Sec. VI, at shear rates where $\dot\gamma\tau$ is large, the body forces due to entanglements $\mathbf{B}_e + \mathbf{B}_0$ tend to zero for uniform systems. At these high shear rates the number of entanglements is essentially zero, and the only remaining interaction forces are due to the "effective potential" W given in Eq. (24). This potential consists of two contributions: the potential V due to core–core interactions and a contribution that is related to the number of entanglements in equilibrium. The forces related to the latter contribution are due to exclusion of the volumes occupied by the coronas, and are sketched in Figs. 4(a) and 5(a) (the dotted lines for which $\dot\gamma\tau = \infty$). As can be seen from Figs. 4(a) and 5(a), the range of these interactions is of the order of $2R_k$, the corona diameter. Since the effective force $-\nabla W$ is antisymmetric in the inter-star separation, unweighted averaging leads to a zero contribution to the shear viscosity for uniform systems in the high shear rate limit. The finite contribution of the effectiveinteractions to the viscosity is due to the shear-induced deformation of the pair-correlation function, which is the weight function with respect to which the averaging must be performed.

Since the high shear viscosity can be expressed in terms of the potential W, we shall refer to the corresponding body force $\mathbf{B}_W$ and viscosity η_W as the "conservative body force" and the "conservative viscosity" respectively. In Sec. XI, an experiment will be discussed that indicates that the shear-thinning behavior of the conservative viscosity plays a role to describe the shear-rate dependence of the high shear-rate branch of the flow curve.

The increasing stress with increasing shear rate due to the effective interactions as described by η_W is essential to describe shear-banding. Since the entanglement contributions to the stress tend to zero at high shear rates, without the high shear-rate branch stresses would tend to zero and there would be no stabilization of the high shear-rate band in a shear banding system.

Consider $\mathbf{B}_W$ as defined in Eq. (23). On the microscopic scale set by the range of V and n_0, the pair-correlation function has the form,

$$\begin{aligned} g(\mathbf{r},\mathbf{r}',t\,|\,[\rho,\dot\gamma]) = g_0(\mathbf{r},\mathbf{r}',t\,|\,[\rho,\dot\gamma]) \\ + \hat{\mathbf{R}}\cdot\hat{\mathbf{E}}\cdot\hat{\mathbf{R}}\, g_1(\mathbf{r},\mathbf{r}',t\,|\,[\rho,\dot\gamma]), \end{aligned} \tag{51}$$

where $\mathbf{R} = \mathbf{r}' - \mathbf{r}$ is the distance between two stars, $\hat{\mathbf{R}}$ is the unit vector in that direction and $\hat{\mathbf{E}}$ is the symmetric part of the velocity gradient tensor, with the hat indicating that the shear rate is divided out. In Eq. (51) we denoted the functional

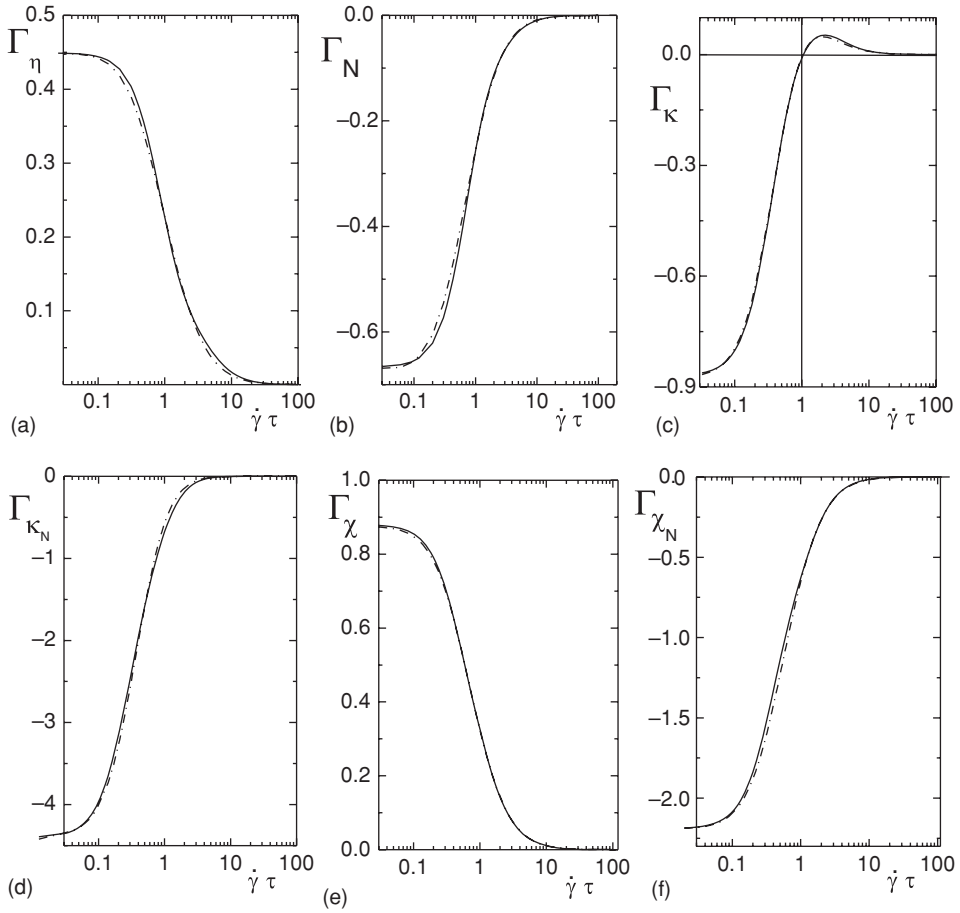

FIG. 6. The dimensionless Γ's as defined in Eq. (B4) as a function of the dimensionless shear rate $\dot{\gamma}\tau$. The dashed-dotted lines are numerical results, where the integrals in Eq. (B4) are evaluated with an accuracy of about 1%, and the solid lines are the Padé approximants in Eq. (50).

dependence of g on the possibly inhomogeneous density and shear rate explicitly. The contribution $g_0 = g^{\text{eq}} + \Delta g_0$ is the sum of the equilibrium pair-correlation function g^{eq} and the isotropic shear-induced distortion Δg_0, while the second term describes the induced anisotropy of the pair-correlation function. Note that, in the absence of shear flow, the pair-correlation function for the very small distances under consideration relaxes to equilibrium very much faster than the time scale on which the large scale density gradients evolve. Even within an inhomogeneous, nonequilibrium situation, we can therefore assume local equilibrium for the pair-correlation function g^{eq} that contributes to g_0. Since the shear rate and density vary only very little over the small distances under consideration, the density $\rho(\mathbf{r}', t)$ can be Taylor expanded around $\mathbf{r}$ to leading order in gradients,

$$\rho(\mathbf{r}', t) = \rho(\mathbf{r}, t) + \mathbf{R} \cdot \nabla \rho(\mathbf{r}, t). \tag{52}$$

Furthermore, the various contributions to the pair-correlation functions are approximately equal to the pair-correlation functions in an isotropic system, but with a density and shear rate in between the positions $\mathbf{r}$ and $\mathbf{r}'$. For example,

$$g_0(\mathbf{r}, \mathbf{r}', t \,|\, [\rho, \dot{\gamma}]) = \bar{g}_0(R \,|\, \bar{\rho}, \bar{\dot{\gamma}}),$$
$$\text{with } \bar{\rho} = \rho(\tfrac{1}{2}(\mathbf{r} + \mathbf{r}'), t) \quad \text{and} \quad \bar{\dot{\gamma}} = \dot{\gamma}(\tfrac{1}{2}(\mathbf{r} + \mathbf{r}'), t), \tag{53}$$

where the overbar on g_0 indicates that this is the correlation function of a system with homogeneous density and shear rate. Within a leading order gradient expansion, it is thus found that,

$$g_0(\mathbf{r}, \mathbf{r}', t \,|\, [\rho, \dot{\gamma}]) = \bar{g}_0(R \,|\, \rho, \dot{\gamma}) + \frac{1}{2} \frac{\partial \bar{g}_0(R \,|\, \rho, \dot{\gamma})}{\partial \rho} \mathbf{R} \cdot \nabla \rho + \frac{1}{2} \frac{\partial \bar{g}_0(R \,|\, \rho, \dot{\gamma})}{\partial \dot{\gamma}} \mathbf{R} \cdot \nabla \dot{\gamma}, \tag{54}$$

and similar for g_1. Substitution of Eqs. (52) and (53) into Eq. (23) for $\mathbf{B}_W$, and performing the angular integrations gives,

$$\mathbf{B}_W(\mathbf{r}, t) = -\left[\frac{\partial P_0(\rho, \dot{\gamma})}{\partial \rho} - k_B T\right] \nabla \rho - \frac{\partial P_0(\rho, \dot{\gamma})}{\partial \dot{\gamma}} \nabla \dot{\gamma} - \frac{\partial P_1(\rho, \dot{\gamma})}{\partial \rho} \hat{\mathbf{E}} \cdot \nabla \rho - \frac{\partial P_1(\rho, \dot{\gamma})}{\partial \dot{\gamma}} \hat{\mathbf{E}} \cdot \nabla \dot{\gamma}, \tag{55}$$

up to leading order in spatial gradients. This can also be written as

$$\mathbf{B}_W(\mathbf{r}, t) = -\nabla [P_0(\rho, \dot{\gamma}) - \rho k_B T] - \hat{\mathbf{E}} \cdot \nabla P_1(\rho, \dot{\gamma}), \tag{56}$$

where,

$$P_0(\rho, \dot{\gamma}) = \rho k_B T - \frac{2\pi}{3} \rho^2 \int_0^\infty dR\, R^3 \frac{dW(R)}{dR} \bar{g}_0(R \,|\, \rho, \dot{\gamma}), \tag{57}$$

and,

$$P_1(\rho,\dot\gamma) = -\frac{4\pi}{15}\rho^2\int_0^\infty dR\,R^3\frac{dW(R)}{dR}\bar g_1(R\,|\,\rho,\dot\gamma). \tag{58}$$

As before, ρ and $\dot\gamma$ are understood to be functions of position $\mathbf{r}$ and time t. Note that with the neglect of shear-induced changes of the pair-correlation, in which case $\bar g_0$ is the equilibrium correlation function, Eq. (57) is nothing but the pressure.

The distortion of the pair-correlation function is only needed within the present context for small distances, and for hard-spherelike interactions, where entanglements are nonexistent. One can therefore resort to either experimental work on the shear-viscosity of hard spheres and/or experimental and theoretical work on the distortion of the pair-correlation function of hard spheres (see, for example, Refs. 50–54).

The contribution $\mathbf{B}_0$ in Eq. (27) is relatively easily evaluated. With the gradient expansion (52) it is immediately found that,

$$\mathbf{B}_0(\mathbf{r},t) = Q\nabla\rho^2(\mathbf{r},t), \tag{59}$$

where,

$$Q = -\alpha\frac{\pi}{3}\int_0^\infty dR R^3\frac{dn_0^2(R)}{dR}. \tag{60}$$

Since the density varies along the gradient direction, the body force $\mathbf{B}_0$ leads to normal forces. The only additional normal force for homogeneous systems is associated with the normal-stress coefficient in Eq. (42). Since the body force $\mathbf{B}_0+\mathbf{B}_e$ for a uniform suspension vanishes for high shear rates (since then the number of entanglements is zero), the body force $\mathbf{B}_0$ must cancel against the normal body forces arising from $\mathbf{B}_e$ for such high shear rates. An asymptotic analysis of the expression (B4) for Γ_N in Appendix B for high shear rates indeed shows that this is the case. To within the accuracy of the Padé approximation for Γ_N, it follows from Eq. (50) that,

$$Q = \frac{25}{48}\alpha\bar n^2 R_k^3. \tag{61}$$

This concludes the discussion on the high-shear body force $\mathbf{B}_W$ in terms of the shear-distorted pair-correlation function and the body force $\mathbf{B}_0$. The derivation of explicit expressions for the pair-correlation is beyond the scope of this paper and will be considered in a future publication.

IX. THE FINAL FORMS OF THE EQUATIONS OF MOTION

In this section we will gather previously derived results, and state the full set of relations, sufficient to describe rheological response and banding phenomena.

The equation of motion for the number density ρ of stars reads (see Sec. V),

$$\frac{\partial\rho}{\partial t}+\nabla\cdot[\rho\mathbf{v}] = D\nabla^2\rho-\beta D\nabla\cdot\mathbf{B}, \tag{62}$$

where $\mathbf{v}$ is the macroscopic velocity and D is the Einstein diffusion coefficient of a freely diffusing star. The effect of interactions between stars is contained in the body force $\mathbf{B}$. The Navier–Stokes equation for the flow velocity can be written as

$$\rho_0\left\{\frac{\partial\mathbf{v}}{\partial t}+\mathbf{v}\cdot\nabla\mathbf{v}\right\} = \mathbf{B}, \tag{63}$$

where ρ_0 is the overall mass density of the system. We will furthermore assume that the flow is incompressible, which renders ρ_0 constant in the comoving frame, i.e., constant in space and time for an initial state with constant density, and so,

$$\nabla\cdot\mathbf{v} = 0. \tag{64}$$

The body force can be rewritten as a sum of a contribution arising from entanglement forces [see Eq. (65)], which dominates at small shear rates, and a contribution arising from potential interactions [see Eq. (56)], which sets the high shear-rate limit of the body force,

$$\begin{aligned}\mathbf{B} = \frac{\partial}{\partial Y}\Bigg[&\left\{\dot\gamma\eta-\frac{\partial^2\dot\gamma}{\partial Y^2}\kappa+\dot\gamma\frac{\partial^2\rho}{\partial Y^2}\chi\right\}\hat{\mathbf{e}}_x\\&+\left\{\dot\gamma^2 N+\dot\gamma\frac{\partial^2\dot\gamma}{\partial Y^2}\kappa_N+\dot\gamma^2\frac{\partial^2\rho}{\partial Y^2}\chi_N\right.\\&\left.-[P_0(\rho,\dot\gamma)-\rho k_BT-Q\rho^2]\right\}\hat{\mathbf{e}}_y\Bigg],\end{aligned} \tag{65}$$

where the viscosity is equal to

$$\eta = \eta_s+\eta_W+\eta_e. \tag{66}$$

Here we have added the solvent viscosity η_s which only applies in case one deals with polymer solutions. The conservative viscosity is related to P_1 in Eq. (58) as

$$\eta_W = -P_1(\rho,\dot\gamma)/\dot\gamma. \tag{67}$$

Furthermore, N the is normal stress coefficient, κ the shear-curvature viscosity, κ_N the nonlocal normal-stress coefficient, χ the shear-concentration coupling parameter, and χ_N the normal-force concentration-coupling parameter, which are all due to entanglement forces. These response functions are specified in Subsection VII D as functions of the shear rate. Furthermore, P_0 in Eq. (57) is related to the shear-induced distortion of the pair-correlation function. In the absence of an isotropic distortion of the pair-correlation function, P_0 is the equilibrium pressure. The quantity Q in Eq. (72) corrects for the use of the deviation $n-n_0$ in $\mathbf{B}_e$ instead of just n. The above expression for the body force is valid up to leading order in gradients, that is, terms like $|\nabla\dot\gamma|^2$ should be omitted.

Not all terms in the expression (65) are equally important, depending on the particular phenomenon of interest. For gradient banding the shear-curvature contribution is essential to describe the interface between the bands[33–36] and the normal body forces are not important, while for vorticity banding the normal stresses are essential and the shear-curvature viscosity can probably be omitted. For an analysis of the SCC-instability[37] the contributions from terms that describe shear-induced mass transport along the gradient direction is essential. A detailed analysis of such instabilities is beyond the scope of this paper. In Sec. X some preliminary consideration on flow-induces instabilities are made.

X. FLOW INDUCED INSTABILITIES

As is well known the gradient-banding instability occurs when the shear stress of the uniformly sheared system decreases with increasing shear rate. The present theory predicts such an instability, as can be seen from Fig. 7(a). Here, the shear stress $\sigma = \dot{\gamma}\,[\eta_s + \eta_W + \eta_e]$ in units of $\sigma^\star = (\eta_s + \eta_W)/\tau$ is plotted as a function of the shear rate. Here, the conservative viscosity η_W is taken independent of the shear rate. According to the first equation in Eq. (49), the dimensionless shear stress is equal to

$$\frac{\sigma}{\sigma^\star} = \dot{\gamma}\tau[1 + K\Gamma_\eta], \tag{68}$$

where,

$$K = \frac{9}{2} w\tau S\varphi^2/(\eta_s + \eta_W). \tag{69}$$

The conservative viscosity η_W can be calculated from the results in Sec. VIII once an explicit expression for the shear-distorted pair-correlation function is known. This is beyond the scope of this paper, so we will use K as a free parameter. The typical van der Waals looplike behavior, reminiscent of gradient banding, is seen to occur for values of K larger than $\approx$50.

The shear-curvature viscosity κ should be positive within the shear-rate region where $d\sigma/d\dot{\gamma}$ is negative.[33,34] Otherwise very large gradients in the flow velocity are the fastest growing modes during the banding transition, which is unphysical. From Fig. 6(c), however, it can be seen that κ is negative for shear rates below approximately $1/\tau$. As can be seen from Fig. 7(b), the range of shear rates, where κ is negative, is always outside the range where $d\sigma/d\dot{\gamma}$ is negative. The points • in Fig. 7(b) denote the shear rate where $d\sigma/d\dot{\gamma}$ becomes negative, and are seen to lie to the right of the vertical line that marks the shear rate where κ becomes negative. The negative values of κ therefore probably do not pose a problem in describing gradient banding. Under controlled shear-rate conditions, and in the absence of coupling to concentration, the stress Σ_{stat} in the stationary banded state can be found from[33,34]

$$\int_{\dot{\gamma}_-}^{\dot{\gamma}_+} d\dot{\gamma}\,\frac{\dot{\gamma}\,\eta(\dot{\gamma}) - \Sigma_{\rm stat}}{\kappa(\dot{\gamma})} = 0. \tag{70}$$

In a future publication we will investigate the instabilities predicted by the constitutive Eq. (65) in more detail. In addition, the present analysis allows to incorporate coupling to concentration, where the difference in concentration in the bands can be accounted for in the above stress-selection rule.

The expression for **B** in Eq. (65) shows that there is diffusive mass transport that is induced by gradients in the shear rate. Shear-gradient induced mass transport has been considered by Schmitt *et al.*[37] by introducing an unspecified additional shear-rate dependence of the chemical potential. This Ansatz is reproduced from our analysis, when entanglement contributions (including the contribution $\sim Q$) in Eq. (65) are neglected. It is readily found from Eqs. (16) and (65) that,

$$\frac{\partial\rho}{\partial t} = -\nabla\cdot\mathbf{j}, \tag{71}$$

where the mass flux **j** is equal to

$$\mathbf{j} = \rho\mathbf{v} - \beta D\frac{\partial P_0}{\partial\rho}\nabla\rho - \beta D\frac{\partial P_0}{\partial\dot{\gamma}}\nabla\dot{\gamma}, \tag{72}$$

where the "generalized pressure" is given in Eq. (57). This reproduces the Ansatz for the flux that was made by Schmitt *et al.*, and identifies the shear-rate dependent chemical potential that has been introduced in an *ad hoc* manner in Ref. 37. Note that the generalized pressure is shear-rate dependent only through the shear-induced isotropic distortion of the pair-correlation function, which is therefore at the origin of the originally proposed SCC-instability.[37] Note, however, that entanglement body forces also contribute to this type of mass transport, but that these contributions cannot be identified with a generalized pressure.

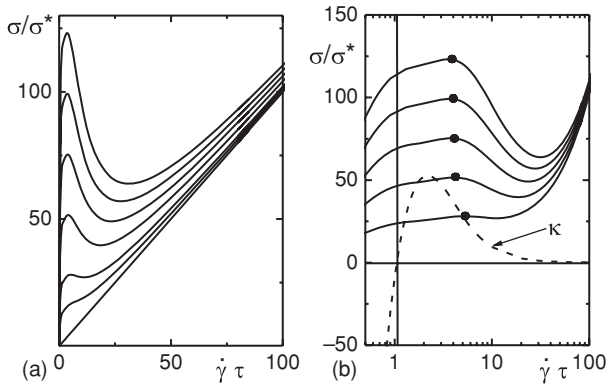

FIG. 7. (a) $\sigma/\sigma^\star$ vs the shear rate for various values of K, from top to bottom: $K = 500$, 400, 300, 200, 100, 50, and 0. (b) The same as in (a) for $K = 500$–100. The points • indicate the shear rate where the shear stress begins to decrease with increasing shear rate. The dashed line is proportional to the shear-curvature viscosity κ.

XI. PRELIMINARY EXPERIMENT

In this section, we discuss an experiment on an entangled star polymer system, and compare the results with our theory. A much more detailed and systematic comparison of experiments with theory is currently underway.

The system consists of polybutadiene stars (1, 4 addition) with a functionality of 122, where each arm has a molar mass of $Ma = 72100$g/mol.[55,56] The stars are dissolved in *n*-tetradecane, a solvent of intermediate quality. At a temperature of 50 °C, the system is close to good solvent conditions.[57] At the concentration in our experiment (6.7wt.%, about 2.2 times its overlapping concentration based on the hydrodynamic volume) the system behaves as a soft colloidal glass. Pictorially, a star of such a high functionality consists of a hard core surrounded by a soft corona, with the capability to entangle with neighboring stars.[38,42] We performed steady shear experiments using an ARES 100 FRTN1-HR fluids rheometer (formerly Rheometric Scientific, TA, USA) with a cone-and-plate geometry (25mm diameter, 0.04rad cone with truncation of 48μm, fixture material being invar, a nickel/copper alloy) and temperature control (500.01 °C) achieved via a circulating ethylene glycol/water mixture.

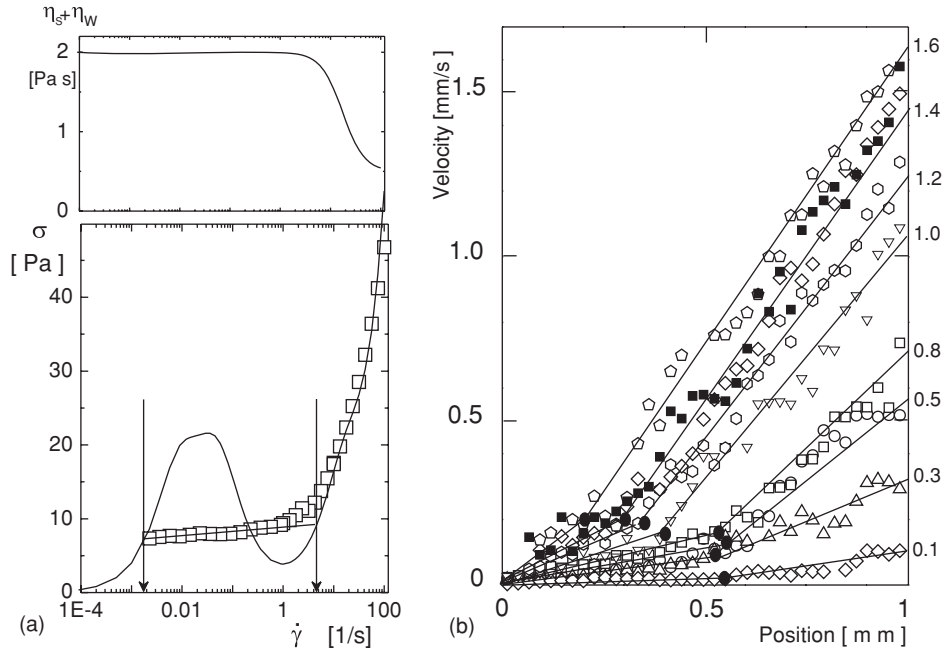

FIG. 8. (a) Shear-rate-dependent stress of the 12 880 star at 6.7wt.% in *n*-tetradecane and 50°C. The open squares are experimental data points, the solid line is theory. The vertical arrows mark the approximate shear-rate range where banding is observed. The insert above (a) is the shear-rate dependence of the conservative viscosity η_W that is necessary to obtain a good comparison between experiment and theory. (b) Corresponding velocity profiles at different applied shear rates which are marked on the right axis in units of $w\,s^{-1}$. The lines through the bands are drawn to guide the eye.

Figure 8(a) depicts the results for the measured stress as a function of shear rate. The shear-rate region where the stress-plateau occurs is indicative for shear-gradient banding. For the same system under the same conditions the velocity profile was measured in a home-made Couette device combined with spatially resolved, heterodyne dynamic light scattering. As demonstrated in Fig. 8(b), for the range of shear rates studied, which correspond to the stress plateau in Fig. 8(a), shear-gradient banding was indeed unambiguously detected, as judged by the heterogeneous velocity profiles with two distinct shear rates. Note that no slip was detected in this system, consistent with expectations.[58] We note that the Couette gap-width of 1mm is sufficiently small to eliminate gap-width effects.[12,13,59]

The solid line in Fig. 8(a) is a comparison with our theory. With the choice of parameters $\tau = 10\,\mathrm{s}$ and $S\varphi^2 = 20\,\mathrm{Pa}$, the van der Waals looplike dependence of the entanglement stress on the shear rate (for the uniformly sheared system) coincides with the region where banding is found, as it should. The higher shear-rate branch ($\dot{\gamma} \gtrsim 3\,\mathrm{s}^{-1}$) could be reproduced by assuming a shear-thinning conservative viscosity of the form $\eta_s + \eta_W = (600 + 0.5\dot{\gamma}^2)/(300 + \dot{\gamma}^2)$, with $\eta_s + \eta_W$ in units Pas and $\dot{\gamma}$ in units s^{-1}. A shear-rate independent η_W does not reproduce the high shear-rate part of the flow curve. The conservative viscosity shear thins from 2Pas for small shear rates to 0.5Pas at very high shear rates, and thinning occurs at a shear rate of about $10\,\mathrm{s}^{-1}$, as can be seen from the insert above Fig. 8(a). The correspondence between this single experiment and theory is at most an indication that there is some truth in our theory. A much more detailed comparison with systematic experiments should be made to validate the accuracy of our theory.

XII. SUMMARY AND CONCLUSIONS

A Smoluchowski equation is formulated for the probability density function of the position coordinates and the number of entanglements of polymerlike particles. The phrase "number of entanglements" has different meanings depending on the system under consideration. For example, for telechelic polymers this is the number of bridges that connect two micelles, and for interpenetrating polymers this is the number contacts between the two polymer chains that can sustain a finite stress for a certain time. The key quantity is the number of entanglements n_0 that exists in equilibrium for a given distance of the center-of-mass of two polymers. The particular choice for n_0 for which explicit expressions for viscoelastic response functions are derived in the present paper is realistic for starlike polymers. For other types of polymers, other choices for n_0 should be made, but the same type of approach can be used to describe their rheology. From the Smoluchowski equation, the equation of motion for the number density of polymers is derived. The same body force that occurs in the Navier–Stokes equation appears in this diffusion equation. The body force has two distinct contributions, one from entanglements and one from core–core interactions. Since the number of entanglements tends to zero at very high shear rates, the latter contribution to the body force determines the high shear viscosity, which must be included to assure realistic predictions for rheology response functions and banding instabilities. The entanglement body force is calculated from a mesoscopic time-evolution equation for the number of entanglements. This body force contains nonlocal contributions which are essential for a realistic description of banding instabilities. In particular, an explicit expression for the shear-curvature viscosity is derived, which prevents formation of

unlimited high spatial gradients in the local suspension velocity during gradient banding, and is essential to describe the interface between the bands in the stationary state. The core–core contribution to the body force gives rise to mass transport induced by spatial gradients in the shear rate, which is related to the shear-induced deformation of the pair-correlation function. The shear-induced distortion of the pair-correlation function is thus shown here to be responsible for a possible SCC-instability.

The two coupled equations for the polymer concentration and the local suspension velocity will be used in a forthcoming paper to investigate various kinds of flow instabilities that can occur in systems where entanglements are important.

ACKNOWLEDGMENTS

We are grateful to J. Roovers for providing the star polymers used and to E. Stiakakis for assistance with characterization. This work was supported in part by the EU, NoE Soft-Comp (Grant No. NMP3-CT-2004-502235) and FP7 NanoDirect (Contract No. CP-FP-213948-2).

APPENDIX A: MATHEMATICAL DETAILS IN THE DERIVATION OF EQ. (38)

As a first step in the derivation of Eq. (38), both the density and the force are expanded up to order Y^3. Let $\mathbf{F}(\mathbf{R}|\dot\gamma+\Delta(Y))$ denote the entanglement force, where the dependence on $\dot\gamma+\Delta(Y)$ is understood to enter through the local velocity $v(Y)=(\dot\gamma+\Delta(Y))Y$ in Eq. (34). An expansion of both the density and the force in the integrand in Eq. (35) leads to

$$\begin{aligned}\mathbf{B}_e=\rho\int d\mathbf{R}\left[\rho+Y\frac{\partial\rho}{\partial Y}+\frac{1}{2}Y^2\frac{\partial^2\rho}{\partial Y^2}+\frac{1}{6}Y^3\frac{\partial^3\rho}{\partial Y^3}\right]\\ \times\left[\mathbf{F}(\mathbf{R}|\dot\gamma)+\Delta(Y)\frac{\partial\mathbf{F}(\mathbf{R}|\dot\gamma)}{\partial\dot\gamma}+\frac{1}{2}\Delta^2(Y)\right.\\ \left.\times\frac{\partial^2\mathbf{F}(\mathbf{R}|\dot\gamma)}{\partial\dot\gamma^2}+\frac{1}{6}\Delta^3(Y)\frac{\partial^3\mathbf{F}(\mathbf{R}|\dot\gamma)}{\partial}\dot\gamma^3\right],\end{aligned}\tag{A1}$$

where $\mathbf{F}(\mathbf{R}|\dot\gamma)$ is the force in Eq. (34) with $v(Y)=Y\dot\gamma$. Here, ρ, $\dot\gamma$, and their spatial derivatives are understood to be taken at the origin. Straightforward multiplication of the various terms, again keeping only terms up to order Y^3 leads to

$$\begin{aligned}\mathbf{B}_e=&\frac{1}{2}\rho^2\frac{\partial\dot\gamma}{\partial Y}\frac{\partial\mathbf{I}_1}{\partial\dot\gamma}+\rho\frac{\partial\rho}{\partial Y}\mathbf{I}_1+\frac{1}{6}\rho\frac{\partial^3\rho}{\partial Y^3}\mathbf{I}_3\\ &+\left\{\frac{1}{24}\rho^2\frac{\partial^3\dot\gamma}{\partial Y^3}+\frac{1}{6}\rho\frac{\partial\rho}{\partial Y}\frac{\partial^2\dot\gamma}{\partial Y^2}+\frac{1}{4}\rho\frac{\partial^2\rho}{\partial Y^2}\frac{\partial\dot\gamma}{\partial Y}\right\}\frac{\partial\mathbf{I}_3}{\partial\dot\gamma}\\ &+\left\{\frac{1}{12}\rho^2\frac{\partial\dot\gamma}{\partial Y}\frac{\partial^2\dot\gamma}{\partial Y^2}+\frac{1}{8}\rho\frac{\partial\rho}{\partial Y}\left(\frac{\partial\dot\gamma}{\partial Y}\right)^2\right\}\frac{\partial^2\mathbf{I}_3}{\partial\dot\gamma^2}\\ &+\frac{1}{48}\rho^2\left(\frac{\partial\dot\gamma}{\partial Y}\right)^3\frac{\partial^3\mathbf{I}_3}{\partial\dot\gamma^3},\end{aligned}\tag{A2}$$

where the abbreviations,

$$\mathbf{I}_n=\int d\mathbf{R}Y^n\mathbf{F}(\mathbf{R}|\dot\gamma),\tag{A3}$$

for $n=1$ and 3 are used for brevity. Noting that,

$$\frac{\partial\dot\gamma}{\partial Y}\frac{\partial\mathbf{I}_1}{\partial\dot\gamma}=\frac{\partial\mathbf{I}_1}{\partial Y},\tag{A4}$$

the first two terms can be written as

$$\frac{1}{2}\rho^2\frac{\partial\dot\gamma}{\partial Y}\frac{\partial\mathbf{I}_1}{\partial\dot\gamma}+\rho\frac{\partial\rho}{\partial Y}\mathbf{I}_1=\frac{\partial}{\partial Y}\left[\frac{1}{2}\rho^2\mathbf{I}_1\right].\tag{A5}$$

Using a similar relation as in Eq. (A4), the last term in Eq. (A2) is rewritten as

$$\begin{aligned}&\frac{1}{48}\rho^2\left(\frac{\partial\dot\gamma}{\partial Y}\right)^3\frac{\partial^3\mathbf{I}_3}{\partial\dot\gamma^3}\\ &=\frac{\partial}{\partial Y}\left[\frac{1}{48}\rho^2\left(\frac{\partial\dot\gamma}{\partial Y}\right)^2\frac{\partial^2\mathbf{I}_3}{\partial\dot\gamma^2}\right]\\ &\quad-\left\{\frac{1}{24}\rho^2\frac{\partial\dot\gamma}{\partial Y}\frac{\partial^2\dot\gamma}{\partial Y^2}+\frac{1}{24}\rho\frac{\partial\rho}{\partial Y}\left(\frac{\partial\dot\gamma}{\partial Y}\right)^2\right\}\frac{\partial^2\mathbf{I}_3}{\partial\dot\gamma^2}.\end{aligned}\tag{A6}$$

Substitution into Eq. (A2) leads to a partial cancelation of the terms $\sim\partial^2\mathbf{I}_3/\partial\dot\gamma^2$. The two remaining terms that are proportional to $\sim\partial^2\mathbf{I}_3/\partial\dot\gamma^2$ in the expression for the body force are

$$\begin{aligned}&\left\{\frac{1}{24}\rho^2\frac{\partial\dot\gamma}{\partial Y}\frac{\partial^2\dot\gamma}{\partial Y^2}+\frac{1}{12}\rho\frac{\partial\rho}{\partial Y}\left(\frac{\partial\dot\gamma}{\partial Y}\right)^2\right\}\frac{\partial^2\mathbf{I}_3}{\partial\dot\gamma^2}\\ &=\frac{\partial}{\partial Y}\left[\left\{\frac{1}{24}\rho^2\frac{\partial^2\dot\gamma}{\partial Y^2}+\frac{1}{12}\rho\frac{\partial\rho}{\partial Y}\frac{\partial\dot\gamma}{\partial Y}\right\}\frac{\partial\mathbf{I}_3}{\partial\dot\gamma}\right]\\ &\quad-\left\{\frac{1}{24}\rho^2\frac{\partial^3\dot\gamma}{\partial Y^3}+\frac{1}{6}\rho\frac{\partial\rho}{\partial Y}\frac{\partial^2\dot\gamma}{\partial Y^2}+\frac{1}{12}\left(\frac{\partial\rho}{\partial Y}\right)^2\frac{\partial\dot\gamma}{\partial Y}\right.\\ &\quad\left.+\frac{1}{12}\rho\frac{\partial^2\rho}{\partial Y^2}\frac{\partial\dot\gamma}{\partial Y}\right\}\frac{\partial\mathbf{I}_3}{\partial\dot\gamma}.\end{aligned}\tag{A7}$$

There is a partial cancelation of terms $\sim\partial\mathbf{I}_3/\partial\dot\gamma$ in this contribution against the similar terms in Eq. (A2) for the body force. The remaining terms $\sim\partial\mathbf{I}_3/\partial\dot\gamma$ in the expression for the body force are

$$\begin{aligned}&\left\{\frac{1}{6}\rho\frac{\partial^2\rho}{\partial Y^2}\frac{\partial\dot\gamma}{\partial Y}-\frac{1}{12}\left(\frac{\partial\rho}{\partial Y}\right)^2\frac{\partial\dot\gamma}{\partial Y}\right\}\frac{\partial\mathbf{I}_3}{\partial\dot\gamma}\\ &=\frac{\partial}{\partial Y}\left[\left\{\frac{1}{6}\rho\frac{\partial^2\rho}{\partial Y^2}-\frac{1}{12}\left(\frac{\partial\rho}{\partial Y}\right)^2\right\}\mathbf{I}_3\right]-\frac{1}{6}\rho\frac{\partial^3\rho}{\partial Y^3}\mathbf{I}_3.\end{aligned}\tag{A8}$$

The last term cancels against the term $\sim\mathbf{I}_3$ in the expression (A2) for the body force. The body force can thus be written as a derivative with respect to Y. Collecting all these terms from

Eqs. (A5) to (A8) thus gives

$$\mathbf{B}_e = \frac{\partial}{\partial Y}\left[\frac{1}{2}\rho^2\mathbf{I}_1 + \frac{1}{48}\rho^2\left(\frac{\partial\dot\gamma}{\partial Y}\right)^2\frac{\partial^2\mathbf{I}_3}{\partial\dot\gamma^2} + \left\{\frac{1}{24}\rho^2\frac{\partial^2\dot\gamma}{\partial Y^2} + \frac{1}{12}\rho\frac{\partial\rho}{\partial Y}\frac{\partial\dot\gamma}{\partial Y}\right\}\frac{\partial\mathbf{I}_3}{\partial\dot\gamma} + \left\{\frac{1}{6}\rho\frac{\partial^2\rho}{\partial Y^2} - \frac{1}{12}\left(\frac{\partial\rho}{\partial Y}\right)^2\right\}\mathbf{I}_3\right]. \quad \text{(A9)}$$

The conclusion from the above calculation is that the body force can be formulated in terms of a stress tensor, even for systems where the density and shear rate are inhomogeneous.

The terms that contain spatial derivatives of the shear rate and/or density are "nonlocal" terms. Not all of these nonlocal contributions to the body force are equally important. A change $\delta\rho$ of the density over a distance R_k, the corona radius, is proportional to a sum of terms of the form $R_k^n\partial^n\rho/\partial Y^n$. Changes of the density over these microscopic distance are assumed to be small. Hence, a term like $R_k^2(\partial\rho/\partial Y)^2$, which measures $(\delta\rho)^2$ can be neglected against terms like $R_k^n\partial^n\rho/\partial Y^n$. This implies that all products of derivatives in the above expression for the body force can be neglected, and hence,

$$\mathbf{B}_e = \frac{\partial}{\partial Y}\left[\frac{1}{2}\rho^2\mathbf{I}_1 + \frac{1}{24}\rho^2\frac{\partial^2\dot\gamma}{\partial Y^2}\frac{\partial\mathbf{I}_3}{\partial\dot\gamma} + \frac{1}{6}\rho\frac{\partial^2\rho}{\partial Y^2}\mathbf{I}_3\right]. \quad \text{(A10)}$$

This concludes the derivation of Eq. (38) for the body force.

APPENDIX B: EVALUATION OF THE SHEAR-RATE DEPENDENCE OF THE ENTANGLEMENT RHEOLOGICAL RESPONSE FUNCTIONS

The response functions in Eqs. (41)–(46) can be written as

$$\eta = \frac{1}{2}\rho^2\frac{1}{\dot\gamma}\int d\mathbf{R}YF_x(\mathbf{R}\,|\,\dot\gamma),$$

$$N = \frac{1}{2}\rho^2\frac{1}{\dot\gamma^2}\int d\mathbf{R}YF_y(\mathbf{R}\,|\,\dot\gamma),$$

$$\kappa = -\frac{1}{24}\rho^2\frac{d}{d\dot\gamma}\int d\mathbf{R}Y^3F_x(\mathbf{R}\,|\,\dot\gamma),$$

$$\kappa_N = \frac{1}{24}\rho^2\frac{1}{\dot\gamma}\frac{d}{d\dot\gamma}\int d\mathbf{R}Y^3F_y(\mathbf{R}\,|\,\dot\gamma), \quad \text{(B1)}$$

$$\chi = \frac{1}{6}\rho\frac{1}{\dot\gamma}\int d\mathbf{R}Y^3F_x(\mathbf{R}\,|\,\dot\gamma),$$

$$\chi_N = \frac{1}{6}\rho\frac{1}{\dot\gamma^2}\int d\mathbf{R}Y^3F_y(\mathbf{R}\,|\,\dot\gamma),$$

where the prime on the spatial integration variables is omitted for convenience. The integrals can be written in dimensionless form, introducing the following dimensionless variables,

$$(x,y,z)=(X,Y,Z)/R_k,\quad r=R/R_k,\quad N_0(r)=n_0(r/R_k)/\bar n. \quad \text{(B2)}$$

The expressions in Eq. (B3) can thus be written as

$$\eta = \frac{1}{2}\rho^2\alpha\tau\bar n^2R_k^3\Gamma_\eta,$$

$$N = \frac{1}{2}\rho^2\alpha\tau^2\bar n^2R_k^3\Gamma_N,$$

$$\kappa = \frac{1}{24}\rho^2\alpha\tau\bar n^2R_k^5\Gamma_\kappa,$$

$$\kappa_N = \frac{1}{24}\rho^2\alpha\tau^2\bar n^2R_k^5\Gamma_{\kappa_N},$$

$$\chi = \frac{1}{6}\rho\alpha\tau\bar n^2R_k^5\Gamma_\chi,$$

$$\chi_N = \frac{1}{6}\rho\alpha\tau^2\bar n^2R_k^5\Gamma_{\chi_N}, \quad \text{(B3)}$$

where the dimensionless Γ's are given by

$$\Gamma_\eta = \frac{-4}{(\dot\gamma\tau)^2}\int_{-\infty}^{\infty}dx\int_0^{\infty}dy\int_0^{\infty}dz\frac{dN_0(r)}{dr}\frac{x}{r}\int_{-\infty}^{x}dx'[N_0(r')-N_0(r)]\exp\left\{\frac{x'-x}{y\dot\gamma\tau}\right\},$$

$$\Gamma_N = \frac{-4}{(\dot\gamma\tau)^3}\int_{-\infty}^{\infty}dx\int_0^{\infty}dy\int_0^{\infty}dz\frac{dN_0(r)}{dr}\frac{y}{r}\int_{-\infty}^{x}dx'[N_0(r')-N_0(r)]\exp\left\{\frac{x'-x}{y\dot\gamma\tau}\right\},$$

$$\Gamma_\kappa = 4\frac{d}{d(\dot\gamma\tau)}\left[\frac{1}{\dot\gamma\tau}\int_{-\infty}^{\infty}dx\int_0^{\infty}dy\int_0^{\infty}dz\frac{dN_0(r)}{dr}\frac{xy^2}{r}\int_{-\infty}^{x}dx'[N_0(r')-N_0(r)]\exp\left\{\frac{x'-x}{y\dot\gamma\tau}\right\}\right], \quad \text{(B4)}$$

$$\Gamma_{\kappa_N} = \frac{-4}{\dot\gamma\tau}\frac{d}{d(\dot\gamma\tau)}\left[\frac{1}{\dot\gamma\tau}\int_{-\infty}^{\infty}dx\int_0^{\infty}dy\int_0^{\infty}dz\frac{dN_0(r)}{dr}\frac{y^3}{r}\int_{-\infty}^{x}dx'[N_0(r')-N_0(r)]\exp\left\{\frac{x'-x}{y\dot\gamma\tau}\right\}\right],$$

$$\Gamma_\chi = \frac{-4}{(\dot\gamma\tau)^2}\int_{-\infty}^{\infty}dx\int_0^{\infty}dy\int_0^{\infty}dz\frac{dN_0(r)}{dr}\frac{xy^2}{r}\int_{-\infty}^{x}dx'[N_0(r')-N_0(r)]\exp\left\{\frac{x'-x}{y\dot\gamma\tau}\right\},$$

$$\Gamma_{\chi_N} = \frac{-4}{(\dot\gamma\tau)^3}\int_{-\infty}^{\infty}dx\int_0^{\infty}dy\int_0^{\infty}dz\frac{dN_0(r)}{dr}\frac{y^3}{r}\int_{-\infty}^{x}dx'[N_0(r')-N_0(r)]\exp\left\{\frac{x'-x}{y\dot\gamma\tau}\right\}.$$

Here, we used the explicit form (34) for the entanglement force, where the new integration variable is $x' = X'/R_k$. These dimensionless quantities are evaluated numerically, and are plotted as a function of the dimensionless shear rate $\dot{\gamma}\tau$ in Fig. 6 as dashed-dotted lines. The solid lines in this figure correspond to the simple forms in Eq. (50) (with $x = \dot{\gamma}\tau$). These approximations capture both the asymptotic behavior for small and large shear rates, as well as the intermediate shear-rate dependence to within a few percent.

[1] J. K. G. Dhont and W. J. Briels, Rheol. Acta **47**, 257 (2008).
[2] R. Besseling, L. Isa, E. R. Weeks, and W. C.K. Poon, Adv. Colloid Interface Sci. **146**, 1 (2009).
[3] J. M. Brader, M. E. Cates, and M. Fuchs, Phys. Rev. Lett. **101**, 138301 (2008).
[4] S. Manneville, Rheol. Acta **47**, 301 (2008).
[5] P. E. Boukany, Y. T. Hu, and S.-Q. Wang, Macomolecules **41**, 2644 (2008).
[6] P. E. Boukany and S.-Q. Wang, J. Rheol. **53**, 73 (2009).
[7] P. Tapadia, S. Ravindranath, and S.-Q. Wang, Phys. Rev. Lett. **96**, 196001 (2006).
[8] S. Ravindranath, S.-Q. Wang, M. Olechnowicz, and R. P. Quirk, Macromolecules **41**, 2663 (2008).
[9] P. T. Callaghan and A. M. Gil, Macromolecules **33**, 4116 (2000).
[10] K. A. Hayes, M. R. Buckley, I. Cohen and L. A. Archer, Phys. Rev. Lett. **101**, 218301 (2008).
[11] K. A. Hayes, M. R. Buckley, H. Qi, I. Cohen, and L. A. Archer, Macromolecules **43**, 4412 (2010).
[12] W. M. Holmes, P. T. Callaghan, D. Vlassopoulos and J. Roovers, J. Rheol. **48**, 1085 (2004).
[13] S. A. Rogers, D. Vlassopoulos and P. T. Callaghan, Phys. Rev. Lett. **100**, 128304 (2008).
[14] S. A. Rogers, P. T. Callaghan, G. Petekidis, and D. Vlassopoulos, J. Rheol. **54**, 133 (2010).
[15] P. Coussot, J. S. Raynaud, F. Bertrand, P. Moucheront, J. P. Guilbaud, H. T. Huynh, S. Jarny, and D. Lesueur, Phys. Rev. Lett. **88**, 218301 (2002).
[16] P. C. F. Möller, S. Rodts, M. A. J. Michels, and D. Bonn, Phys. Rev. E. **77**, 041507 (2008).
[17] L. Bécu, S. Manneville, and A. Colin, Phys. Rev. Lett. **96**, 138302 (2006).
[18] M. Cloitre, R. Borrega, F. Monti, and L. Leibler, Phys. Rev. Lett. **90**, 068303 (2003).
[19] Y. Goutille and J. Guillet, J. Rheol. **46**, 1307 (2002).
[20] A. v. d Noort and W. J. Briels, J. Non-Newtonian Fluid Mech. **152**, 148 (2008).
[21] A. van den Noort and W. J. Briels, Macromol. Theory Simul. **6**, 742 (2007).
[22] M. Doi and S. Edwards, *The Theory of Polymers Dynamics* (Oxford University Press, New York, 1986).
[23] G. Marrucci, J. Non-Newtonian Fluid Mech. **62**, 279 (1996).
[24] J. M. Adams and P. D. Olmsted, Phys. Rev. Lett. **102**, 067801 (2009).
[25] N. A. Spenley, M. E. Cates, and T. C.B. McLeish, Phys. Rev. Lett. **71**, 939 (1993).
[26] S. T. Milner, T. C.B. McLeish, and A. E. Likhtman, J. Rheol. **45**, 539 (2001).
[27] E. Michel, J. Appell, F. Molino, J. Kieffer, and G. Porte, J. Rheol. **45**, 1465 (2001).
[28] J.-F. le Meins and J.-F. Tassin, Macromolecules **34**, 2641 (2001).
[29] J. Sprakel, E. Spruijt, M. A. Cohen Stuart, N. A. M. Besseling, M. P. Lettinga, and J. van der Gucht, Soft Matter **4**, 1696 (2008).
[30] H. Tabuteau, L. Ramos, K. Nakaya-Yaegashi, M. Imai, and C. Ligoure, Langmuir **25**, 2467 (2009).
[31] J. Sprakel, E. Spruijt, M. A. Cohen Stuart, M. A. J. Michels, and J. van der Gucht, Phys. Rev. E **79**, 056306 (2009).
[32] J. Sprakel, E. Spruijt, J. van der Gucht, J. T. Padding, and W. J. Briels, Soft Matter **5**, 4748 (2009).
[33] J. K. G. Dhont, Phys. Rev. E **60**, 4534 (1999).
[34] P. D. Olmsted and C.-Y. D. Lu, Faraday Discuss. **112**, 183 (1999).
[35] C.-Y. D. Lu, P. D. Olmsted, and R. C. Ball, Phys. Rev. Lett. **84**, 642 (2000).
[36] X.-F. Yuan, Europhys. Lett. **46**, 542 (1999).
[37] V. Schmitt, C. M. Marques, and F. Lequeux, Phys. Rev. E **52**, 4009 (1995).
[38] C. N. Likos, Phys. Rep. **348**, 267 (2001).
[39] D. Vlassopoulos, J. Polym. Sci., Part B: Polym. Phys. **42**, 2931 (2004).
[40] W. J. Briels, Soft Matter **5**, 4401 (2009).
[41] A. van den Noort, W. K. den Otter, and W. J. Briels, Europhys. Lett. **80**, 28003 (2007).
[42] M. Daoud and J. P. Cotton, J. Phys. **43**, 531 (1982).
[43] C. N. Likos and H. M. Harreis, Condens. Matter Phys. **5**, 173 (2002).
[44] S. Huissmann, R. Blaak, and C. N. Likos, Macromolecules **42**, 2806 (2009).
[45] J. T. Padding, E. van Ruymbeke, D. Vlassopoulos, and W. J. Briels, Rheol. Acta **44**, 473 (2010).
[46] This expression for the friction force is Faxén's theorem for hard-body spheres, where the gradient contribution is neglected. Here we consider the opposite of hard-body spheres, namely very open starlike polymers. Since the outer parts of the star are penetrable for solvent, the gradient contribution to a similar Faxén's theorem will be much smaller as compared to hard-body spheres, and is therefore neglected.
[47] J. K. G. Dhont, *An Introduction to Dynamics of Colloids* (Elsevier, Amsterdam, 1996).
[48] J. K. G. Dhont, J. Chem. Phys. **105**, 5112 (1996).
[49] P. D. Olmsted and C.-Y. D. Lu, Phys. Rev. E **56**, 55 (1997).
[50] B. J. Ackerson, J. van der Werff, and C. G. de Kruif, Phys. Rev. A **37**, 4819 (1988).
[51] Y. S. Lee and N. J. Wagner, Ind. Eng. Chem. Res. **45**, 7015 (2006).
[52] N. J. Wagner and B. J. Ackerson, J. Chem. Phys. **97**, 1473 (1992).
[53] D. Ronis, Phys. Rev. A **29**, 1453 (1984).
[54] J. K. G. Dhont, J. Fluid Mech. **204**, 421 (1989).
[55] J. Roovers, L.-L. Zhou, P. M. Toporowski, M. van der Zwan, H. Iatrou, and N. Hadjichristidis, Macromolecules **26**, 4324 (1993).
[56] L.-L. Zhou, N. Hadjichristidis, P. M. Toporowski, and J. Roovers, Rubber Chem. Technol. **65**, 303 (1992).
[57] E. Stiakakis, D. Vlassopoulos, B. Loppinet, J. Roovers, and G. Meier, Phys. Rev. E. **66**, 051804 (2002).
[58] M. E. Helgeson, N. J. Wagner, and D. Vlassopoulos, J. Rheol. **51**, 297 (2007).
[59] G. Ovarlez, S. Rodts, P. Coussot, J. Goyon, and A. Colin, Phys. Rev. E **78**, 036307 (2008).